Electronic Supplementary Material (ESI) for Chemical Science.

Isolable Iodosylarene and Iodoxyarene Adducts of Co and Their O-atom Transfer and C-H Activation Reactivity

Ethan A. Hill, Margaret L. Kelty, Alexander S. Filatov, and John S. Anderson*

Table of Contents

1.0 Experimental Section

1.1 Materials and Instrumentation

All manipulations were carried out under a dry N_2 atmosphere using either standard Schlenk technique or in an mBraun Unilab Pro glove box. All chemicals obtained from commercial sources and used as received unless otherwise stated. Solvents were dried on a solvent purification system from Pure Process Technologies before storing over 4Å molecular sieves under N_2. Tetrahydrofuran (THF) was stirred over NaK alloy and passed through a column of activated alumina prior to storing over 4Å sieves under N_2. Iodosylbenzene, Na[$Tp^{Ad,Me}$], $NaBAr^F_4$, $Co(MeCN)_6OTf_2$, and d_4-DHA were prepared following literature procedures.[1–5] Synthesis of K[Tp^{tBu}] followed a literature procedure for the synthesis of Li[Tp^{tBu}] substituting KBH_4 for $LiBH_4$, all other synthetic procedures were followed as reported.[6]

The iodoxyarene, $^sPhIO_2$, was prepared by allowing a concentrated solution of ^sPhIO (300 mg, 0.88 mmol) in 10 mL of DCM to stir until the yellow color had dissipated, approximately three days. The resulting white precipitate was collected by filtration and washed several times with cold DCM and Et_2O before drying under vacuum to yield a white powder (212 mg, 67%). The spectroscopic features of this material matched a previous literature report.[7]

UV-vis spectra were recorded on either a Thermo Scientific Evolution 300 spectrometer with the VISIONpro software suite or a Cary 5000 UV/Vis/IR UMA spectrophotometer located in the UChicago MRSEC Materials Preparation and Measurement Laboratory. IR spectra were recorded on a Bruker Tensor II spectrometer with the OPUS software suite. All IR samples were prepared as KBr pellets in a homemade press. EPR spectra were recorded on a Bruker Elexsys E500 spectrometer with an Oxford ESR 900 X-band cryostat and a Bruker Cold-Edge Stinger. NMR spectra for ^1H, ^{19}F, and $^{31}P\{^1H\}$ were recorded on either Bruker DRX-400 or AVANCE-500 spectrometers. Integrations of paramagnetic species are relative only to paramagnetic peaks, therefore in reported spectra below, resonances from diamagnetic protons, such as BAr^F_4 counter ions, were not given integral values. Combustion analysis performed by Midwest Microlab. Mass spectra were recorded on an Agilent 6130 ESI LC-MS by direct injection. Organic products identified by GC-MS using an Agilent 7890B GC equipped with an Agilent HP-5MS column coupled to an Agilent 5977A EI-MS. Isotope patterns compared to the NIST library to confirm assignments.

1.2 Complex Synthesis and Characterization

[$CoTp^{Ad,Me}(^sPhIO)][BAr^F_4]$ (1). To a solution of **4** (50 mg, 0.058 mmol) in 6 mL of Et_2O was added $NaBAr^F_4$ (54 mg, 0.061 mmol) followed by ^sPhIO (21 mg, 0.060 mmol). This mixture was allowed to stir for ~15 min before filtering through Celite. The resulting blue solution was then layered under petroleum ether in several portions before placing in a −35 °C freezer for several days to afford blue clumps of crystalline material (78 mg, 76%). Single crystals were grown by slow diffusion of petroleum ether into a concentrated solution in DCM at −35 °C over several days. UV-vis, nm in Et_2O 25 °C (ε, $M^{-1}cm^{-1}$): 572 (330), 634 (610), 652 (580), and 995 (120). IR (cm^{-1}): 2909 (s), 2855 (m), 2564 (m, ν_{B-H}), 1875 (w), 1835 (w), 1781 (w), 1656 (m), 1544 (s), 1479 (m), 1452 (m), 1425 (m), 1355 (m), 1280 (m), 1182 (m), 1130 (m), 939 (m), 887 (m), 840 (m), 792 (m), 748 (m), 715 (w), 680 (m), 667 (m), 642 (m). ^1H NMR ($CDCl_3$, 400 MHz): δ 78.00 (s, 3H), 18.86 (d, 1H), 18.37 (s, 9H), 14.61 (s, 1H), 10.06 (s, 1H), 7.75 (s, BAr^F_4), 7.57 (s, BAr^F_4), 6.09 (br, 18H), 2.77 (s, 9H), 2.44 (s, 9H), 1.51 (s, 9H), 0.80 (s, 9H). ^{19}F NMR ($CDCl_3$, 470 MHz): δ −62.6. Anal. Calc. for $C_{84}H_{83}N_6O_3SB_2F_{24}ICo$: C 52.55, H 4.36, N 4.38, Found: C 52.37, H 4.43, N 4.08.

[$CoTp^{tBu}(^sPhIO)][BAr^F_4]$ (2). To a solution of **5** (40 mg, 0.068 mmol) in 6 mL of Et_2O was added $NaBAr^F_4$ (66.2 mg, 0.075 mmol) and ^sPhIO (25.4 mg, 0.075 mmol). After 20 minutes of stirring the blue solution was filtered through Celite and dried under vacuum. The resulting blue solid was redissolved in DCM before filtering through Celite to remove insoluble material and dried under vacuum once more. Finally, the blue residue was washed three times with petroleum ether and dried under vacuum to yield a blue powder (93 mg, 83%) which could be used without further purification. Single crystals suitable for X-ray diffraction were grown from a concentrated Et_2O solution layered with hexamethyldisyloxane and stored

at −35 °C for 7 days. UV-vis, nm in Et_2O, 25 °C (ε, $M^{-1}cm^{-1}$): 576 (350), 634 (700), 652 (680), 946 (96). IR (cm^{-1}): 3156 (m), 2970 (s), 2876 (w), 2498 (w, ν_{B-H}), 1660 (w), 1611 (m), 1503 (m), 1398 (m), 1355 (s), 1279 (s), 1127 (s), 932 (m), 887 (m), 714 (m). ^{1}H NMR ($CDCl_3$, 500 MHz): δ 77.53 (s, 3H), 31.03 (s, 3H), 16.61 (s, 1H), 7.89 (br, 1H), 7.67 (s, BAr^F_4), 7.47 (s, BAr^F_4), 6.50 (br, 1H), 6.00 (br, 27H), 0.77 (s, 9H), −6.45 (br, 1H), −10.01 (br, 1H). ^{19}F NMR ($CDCl_3$, 470 MHz): δ −62.6. Anal. Calc. for $C_{63}H_{59}B_2CoF_{24}IN_6O_3S$: C 46.04, H 3.62, N 5.11. Found: C 46.06, H 3.74, N 4.93.

[$CoTp^{tBu}$(^{s}$PhIO_2$)][BAr^F_4] (3). To a solution of **5** (73 mg, 0.12 mmol) in 6 mL of Et_2O was added $NaBAr^F_4$ (116 mg, 0.13 mmol) and ^{s}$PhIO_2$ (47 mg, 0.13 mmol). After 20 minutes of stirring, the blue solution was filtered through Celite and dried under vacuum. The resulting blue residue was redissolved in minimal DCM and filtered once more through Celite to remove insoluble material before drying under vacuum to yield a blue powder (138 mg, 67%) which could be used without further purification. Single crystals of **3** were grown from a concentrated solution of diethyl ether layered beneath petroleum ether at −35 °C over several days. UV-vis, nm in Et_2O, 25 °C (ε, $M^{-1}cm^{-1}$): 580 (sh, 530), 635 (820), 950 (140). IR data (cm^{-1}): 3159 (m), 2972 (m), 2500 (w, ν_{B-H}), 1661 (w), 1612 (w), 1504 (m), 1399 (m), 1355 (s), 1279 (s), 1127 (s), 1029 (m), 713 (m). ^{1}H NMR ($CDCl_3$, 500 MHz): δ 82.85 (s, 3H), 20.38 (s, 3H) 10.89 (s, 1H), 9.81 (br, 27H), 7.48 (s, BAr^F_4), 7.31 (s, BAr^F_4), 6.41 (s, 1H), 3.74 (s, 1H), −5.11 (s, 1H), −23.69 (br, 1H). ^{19}F NMR ($CDCl_3$, 470 MHz): δ −62.6. Anal. Calc. for $C_{63}H_{59}B_2CoF_{24}IN_6O_4S$ C 45.59, H 3.58, N 5.06, Found: C 45.57, H 3.59, N 5.04.

[$CoTp^{Ad,Me}$(OTf)] (4). To a solution of [$NaTp^{Ad,Me}$] (500 mg, 0.73 mmol) in 20 mL of DCM was added $Co(MeCN)_6(OTf)_2$ (445 mg, 0.74 mmol). The mixture was allowed to stir for 24 h before filtering through a fine fritted glass funnel to remove insoluble materials and yield a deep blue solution. The volatiles were removed *in vacuo* and the resulting blue residue was taken up in boiling petroleum ether with minimal THF (~5 mL, 9:1 ratio of petroleum ether to THF) before filtering hot through Celite. The resulting solution was cooled to room temperature whereupon dark blue crystals began to form. After cooling, crystallization was driven to near completion by storing in a −35 °C freezer overnight. The supernatant was then decanted away from the crop of blue crystals which were rinsed with cold petroleum ether before drying *in vacuo* to obtain dark blue crystalline material (480 mg, 76%). Single crystals suitable for X-ray diffraction were grown from slow diffusion of petroleum ether into a concentrated THF solution at −35 °C over the course of several days. UV-vis, nm in DCM 25 °C (ε in $M^{-1}cm^{-1}$): 512 (sh, 90), 546 (260), 556 (270), 620 (420), 630 (400), and 1030 (70). IR (cm^{-1}): 2910 (s), 2850 (m), 2564 (m, ν_{B-H}), 1653 (m), 1546 (s), 1427 (m), 1342 (m), 1230 (m), 1200 (m), 1098 (m), 1067 (m), 1014 (m), 862 (m), 791 (m), 750 (m), 682 (m), 631 (m). ^{1}H NMR ($CDCl_3$, 400 MHz): δ 79.0 (3H), 15.9 (9H), 8.2 (18H), 2.9 (9H), 2.2 (9H), 0.0 (9H), −4.5 (1H). ^{19}F NMR ($CDCl_3$, 470 MHz): δ −7.4. Anal. Calc. for $C_{43}H_{58}N_6O_3F_3BSCo$: C 59.65, H 6.75, N 9.71, Found: C 59.92, H 6.74, N 9.03. Anal. Calc. for $C_{47}H_{66}N_6O_4F_3BSCo$ (one additional molecule of THF included): C 60.19, H 7.09, N 8.96, Found: C 59.90, H 6.77, N 8.58. Elemental analysis for **4** is slightly but consistently off from the predicted value for the molecular formula. We believe that this variability may be due to solvent inclusion from crystallization. As can be seen, the experimental values match well with those predicted for a mono-THF solvate.

[$CoTp^{tBu}$OTf] (5). To a solution of K[Tp^{tBu}] (400 mg, 0.95 mmol) in 18 mL DCM was added $Co(MeCN)_6OTf_2$ (574 mg, 0.95 mmol). After stirring for 24 hours, the reaction was filtered through a medium fritted glass funnel and the resulting blue filtrate was dried under vacuum. The residue was dissolved in boiling petroleum ether and THF mixture and filtered hot before being cooled to room temperature and stored at −35 °C for one day to yield microcrystalline product (357 mg, 64%). Single crystals suitable for X-ray diffraction were grown from a concentrated Et_2O solution layered with petroleum ether and stored at −35 °C for two days. UV-vis, nm in Et_2O 25 °C (ε, $M^{-1}cm^{-1}$): 574 (330), 616 (580), 956 (70). IR (cm^{-1}): 3137 (m), 2967 (s), 2869 (m), 2516 (w, ν_{B-H}), 1636 (w), 1503 (s), 1396 (s), 1258 (s), 1194 (s), 1170 (m), 1058 (m), 1033 (m), 788 (m), 735 (m), 639 (m). ^{1}H NMR ($CDCl_3$, 500 MHz): δ 79.91 (s,

3H), 23.64 (s, 3H), 9.79 (br, 27H), −21.07 (br, 1H). ^{19}F NMR ($CDCl_3$, 470 MHz): δ −30.0 (s). Anal. Calc. for $C_{22}H_{34}BCoF_3N_6O_3S$: C 44.84, H 5.82, N 14.26. Found: C 44.79, H 5.73, N 14.27.

[CoTp^{Ad,Me}H(pyr^{Ad,Me})OTf][BAr$^F_4$] (6). To a solution of **1** (25 mg, 0.013 mmol) in 3 mL of Et_2O was added $ScOTf_3$ (64 mg, 0.13 mmol). The suspension was stirred overnight during which time a purple solution formed which was filtered through Celite and layered under petroleum ether at −35 °C. Single crystals formed from this solution over the course of several days which were suitable for X-ray diffraction studies (17 mg). Due to the complicated ^{1}H NMR spectrum, peaks were not assigned and relative integrations were reported only for well isolated peaks. UV-vis, nm, 25 °C in Et_2O: 542, 596, ~1090. ^{1}H NMR ($CDCl_3$, 400 MHz): δ 48.11 (s, 2H), 38.69 (s, 1H), 36.91 (s, 6H), 12.53 (d, 2H), 8.65 (s, 6H), 7.90 (s, BAr^F_4), 7.61 (s, BAr^F_4), 6.58 (d, 9H), 6.17 (s, 1H), 5.07, 4.77, 4.58, 2.38 (s, 3H), 2.09 (s), 1.89 (s), 0.22 (s), −0.43 (s br), −0.46 (s), −2.89 (s, 6H), −9.52 (br), −11.67 (br).

2.0 Spectroscopic Data

2.1 IR Spectra

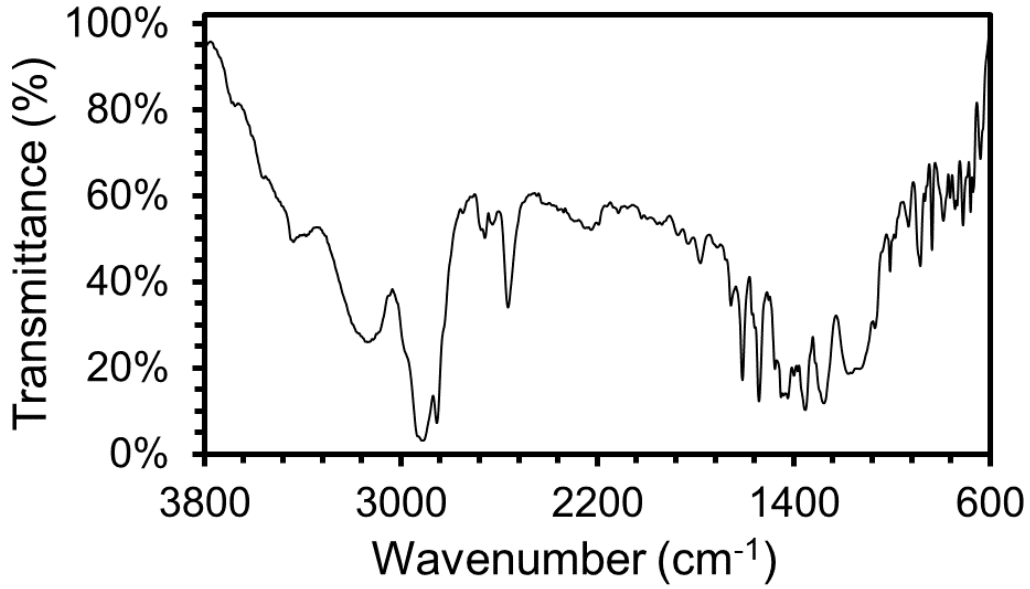

Figure S1. Vibrational spectrum of **1** as KBr pellet (see text above for specific peak values).

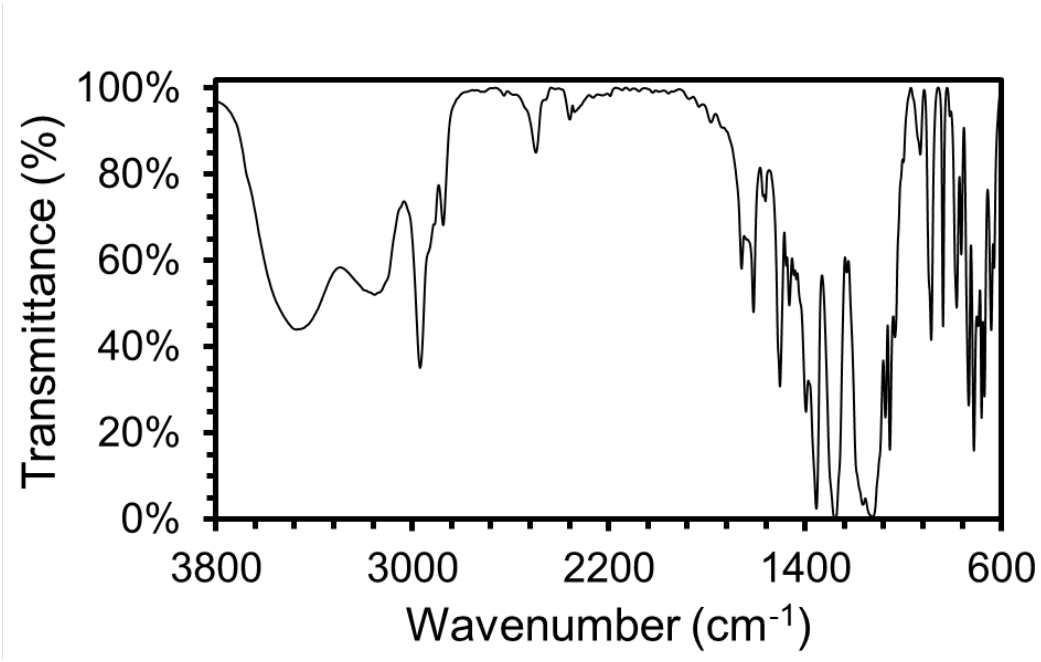

Figure S2. Vibrational spectrum of **2** as KBr pellet (see text above for specific peak values).

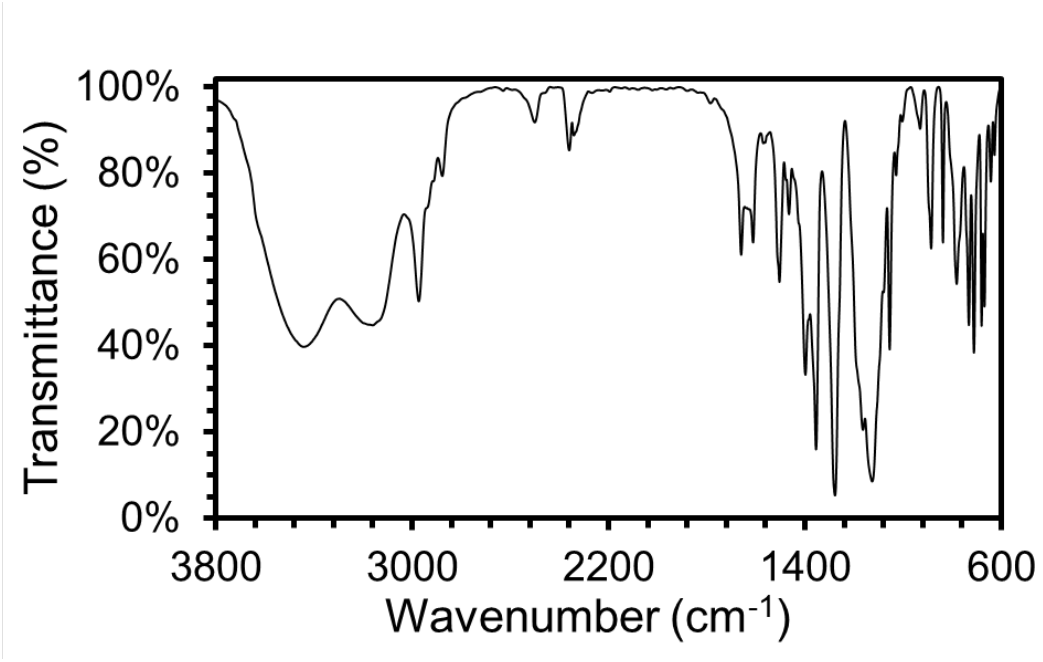

Figure S3. Vibrational spectrum of **3** as KBr pellet (see text above for specific peak values).

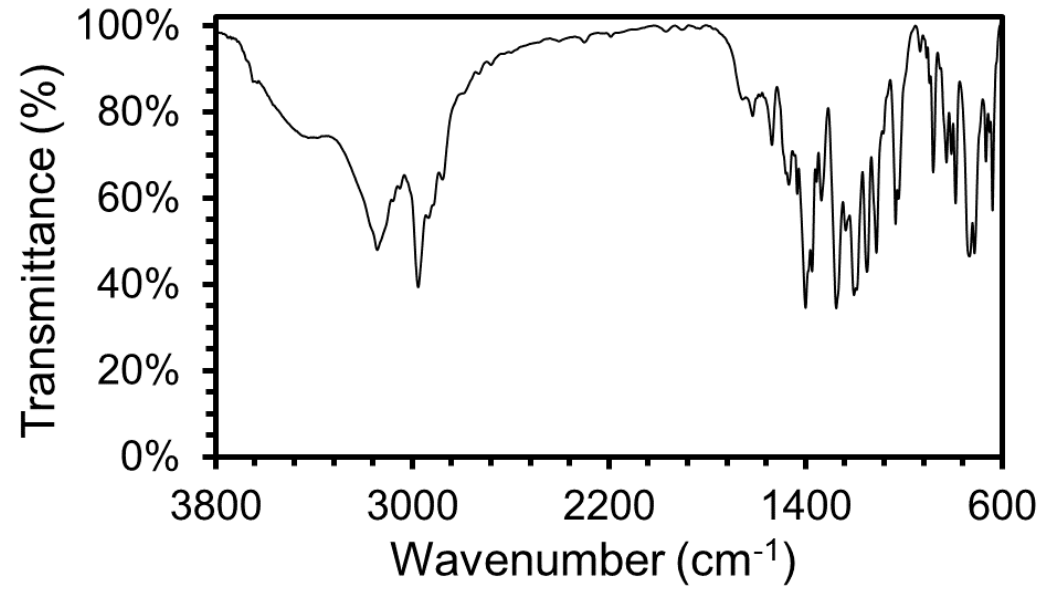

Figure S4. Vibrational spectrum of **4** as KBr pellet (see text above for specific peak values).

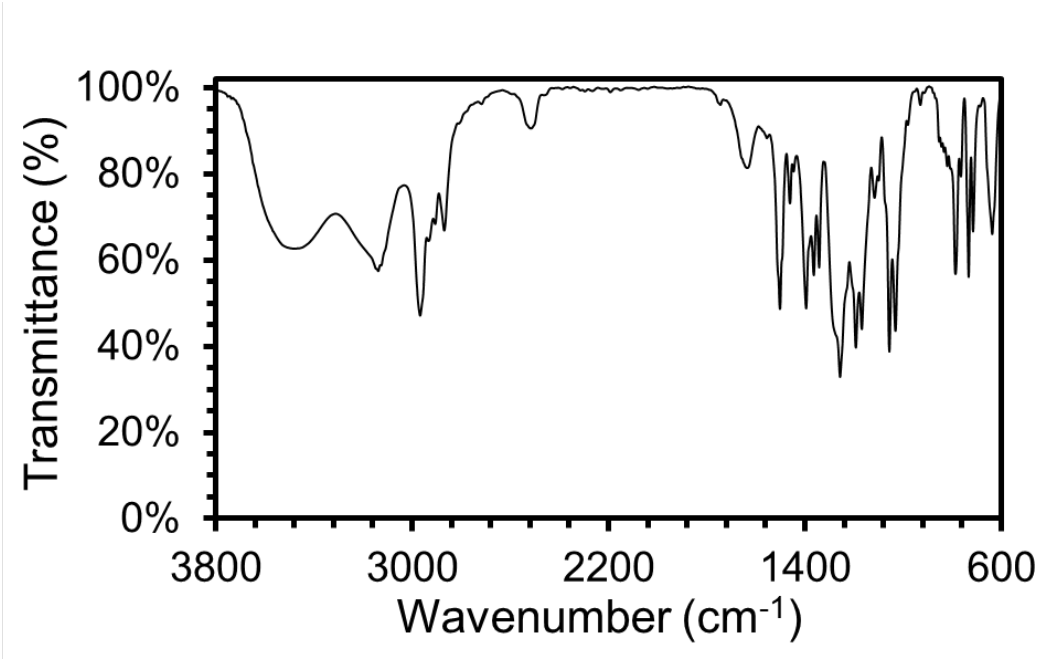

Figure S5. Vibrational spectrum of **5** as KBr pellet (see text above for specific peak values).

2.2 UV-vis Spectra

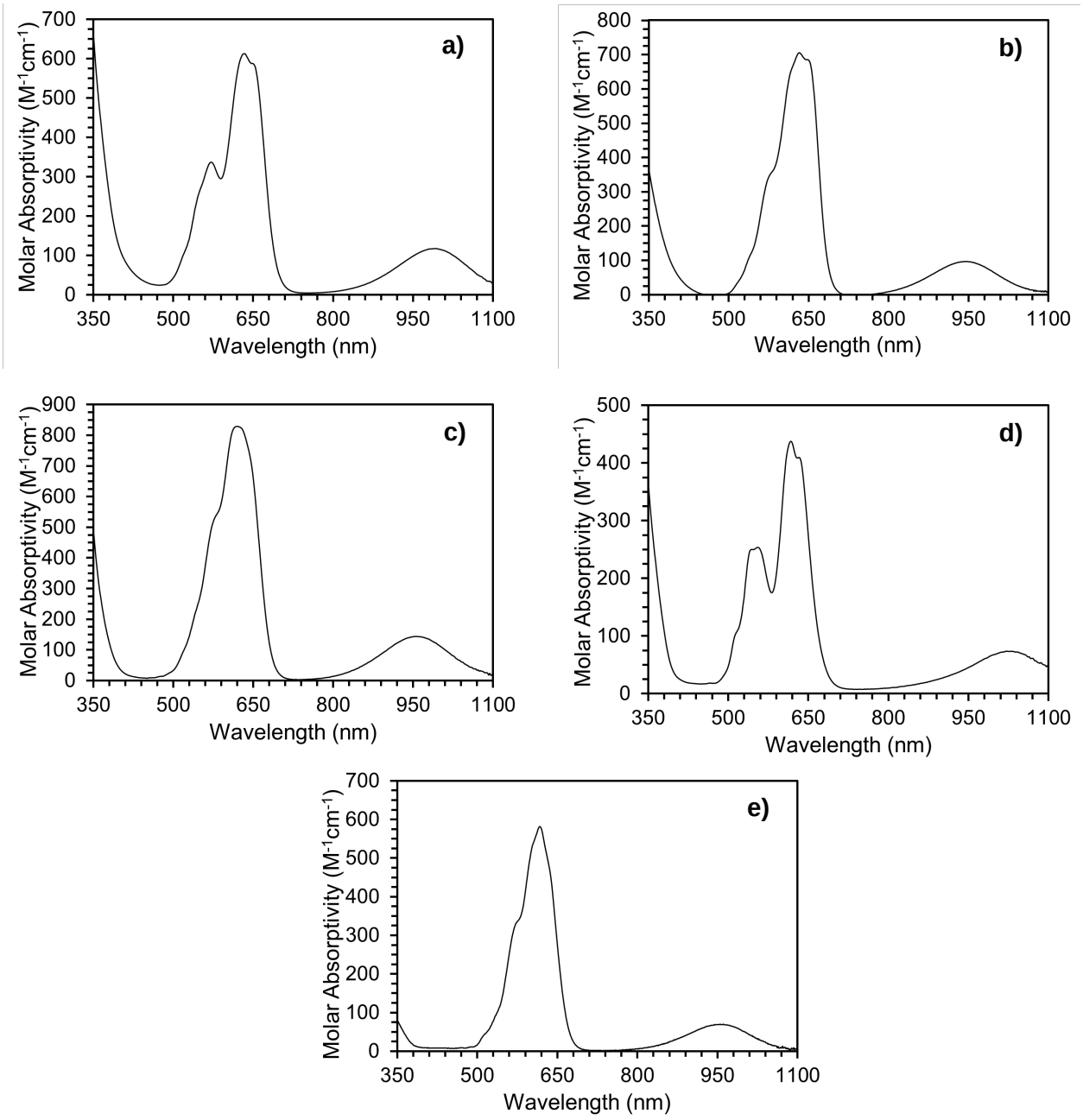

Figure S6. UV-vis spectra for complexes **1** (a), **2** (b), **3** (c), **4** (d), and **5** (e). Complexes **1**-**3** and **5** are solutions in Et_2O while **4** is a solution in DCM, all recorded at room temperature. See text above for detailed peak positions and absorptivity values.

2.3 NMR Spectra

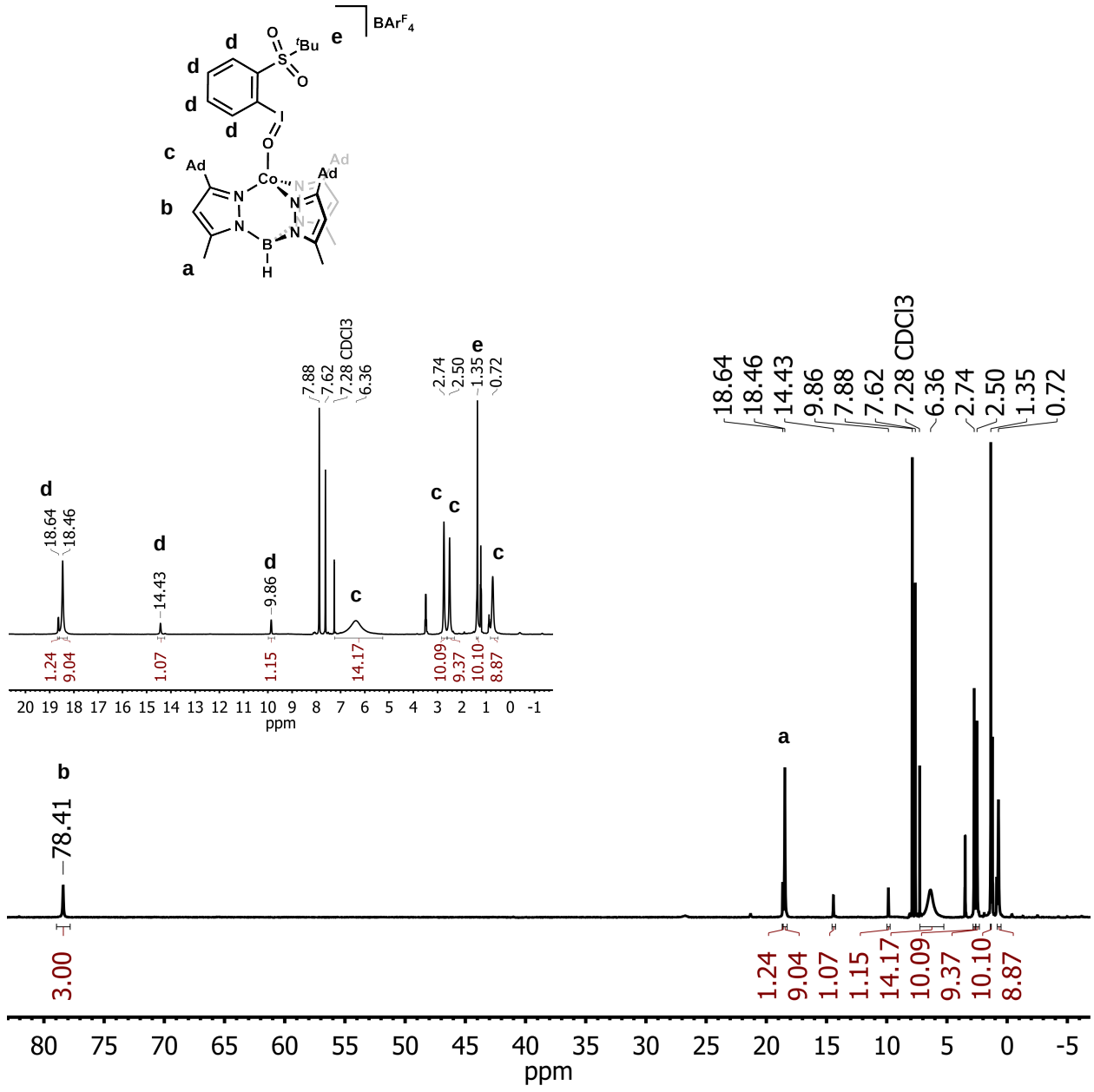

Figure S7. The ^{1}H NMR spectrum of **1** in $CDCl_3$. Inset is expanded near the diamagnetic region to show details. Note: Residual solvent and BAr^F_4 resonances not labeled.

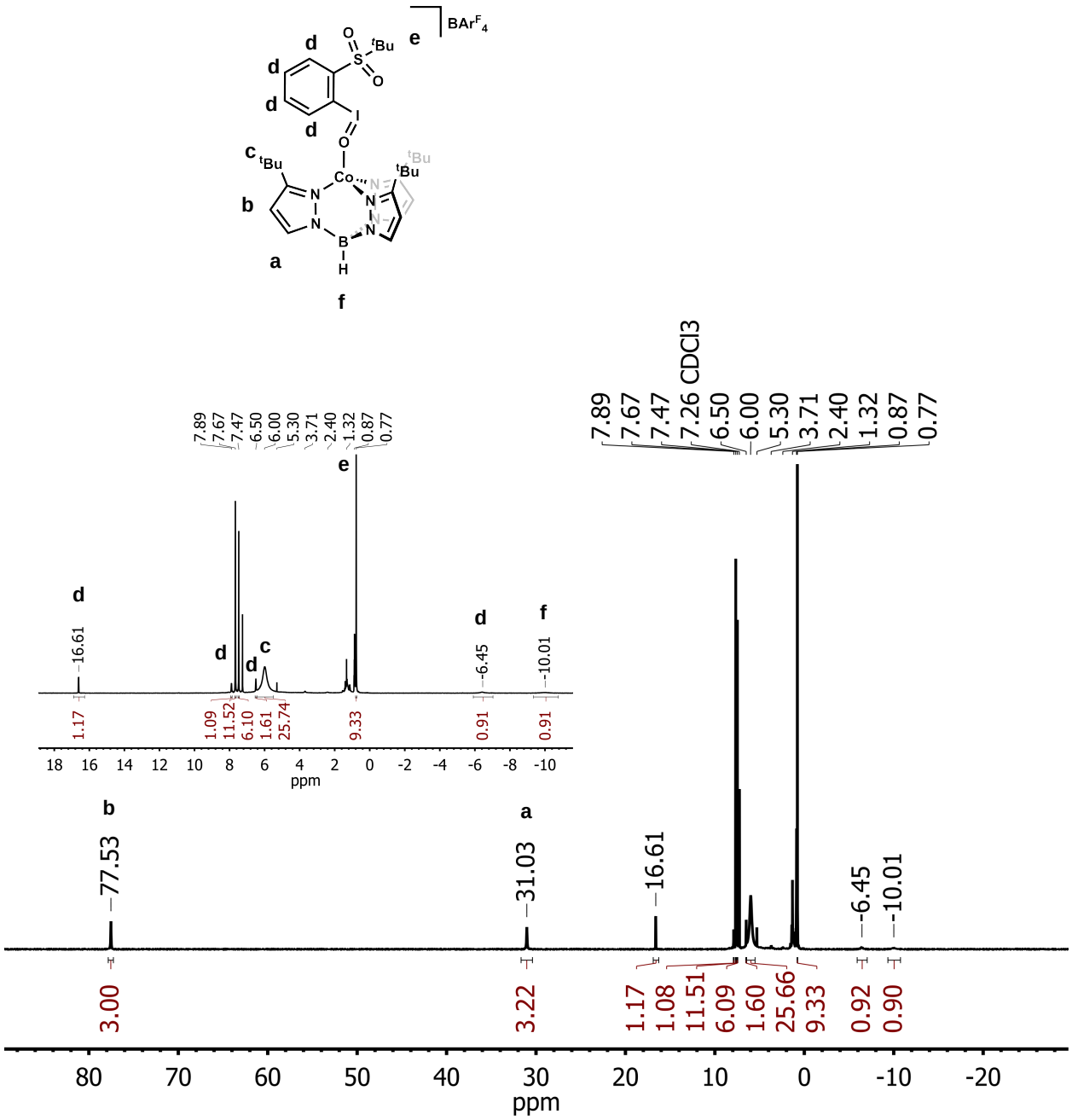

Figure S8. The ^{1}H NMR spectrum of **2** in $CDCl_3$. Inset is expanded near the diamagnetic region to show details. Note: Residual solvent and BAr^F_4 resonances not labeled.

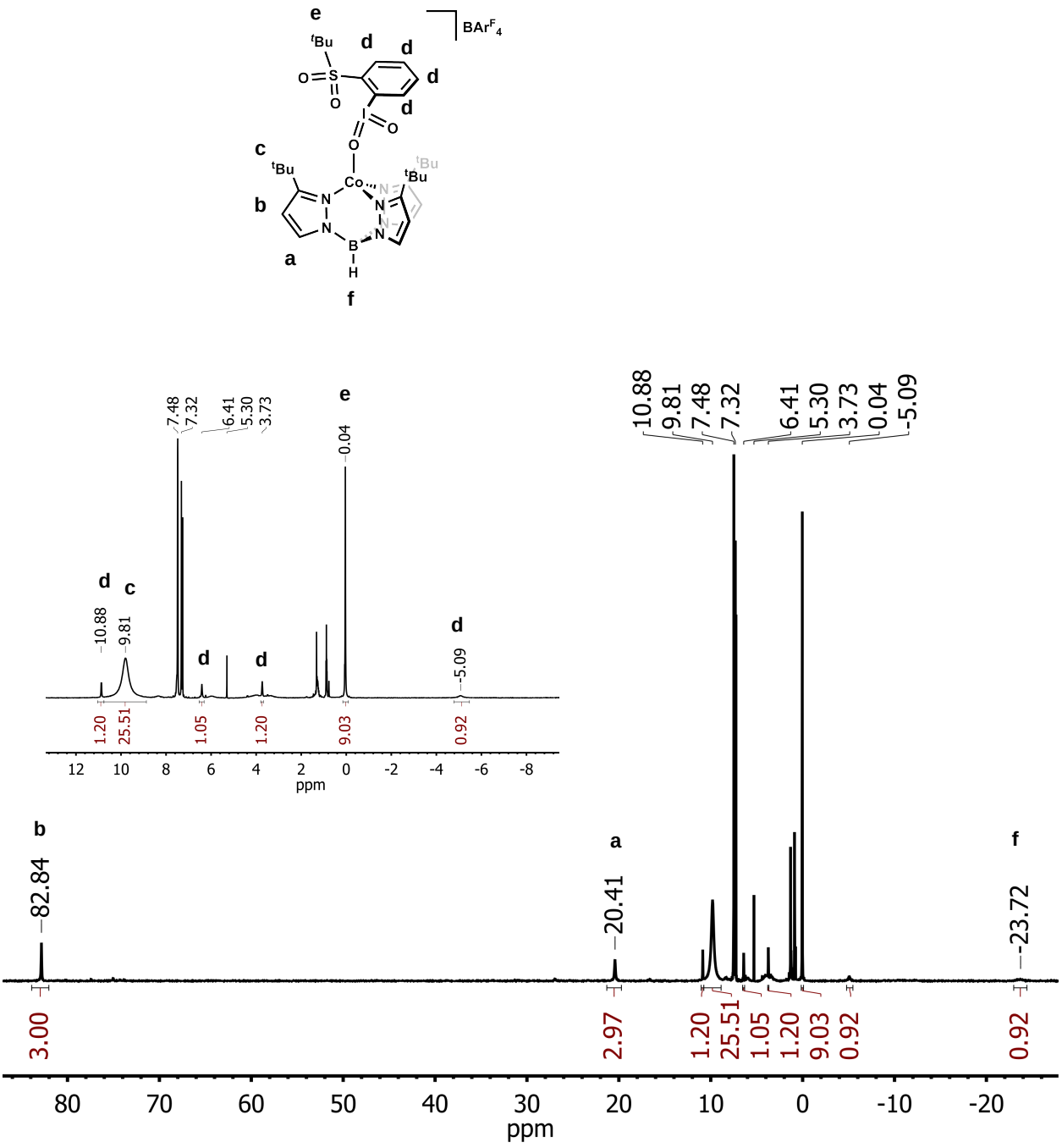

Figure S9. The ^{1}H NMR spectrum of **3** in $CDCl_3$. Inset is expanded near the diamagnetic region to show details. Note: Residual solvent and BAr^F_4 resonances not labeled.

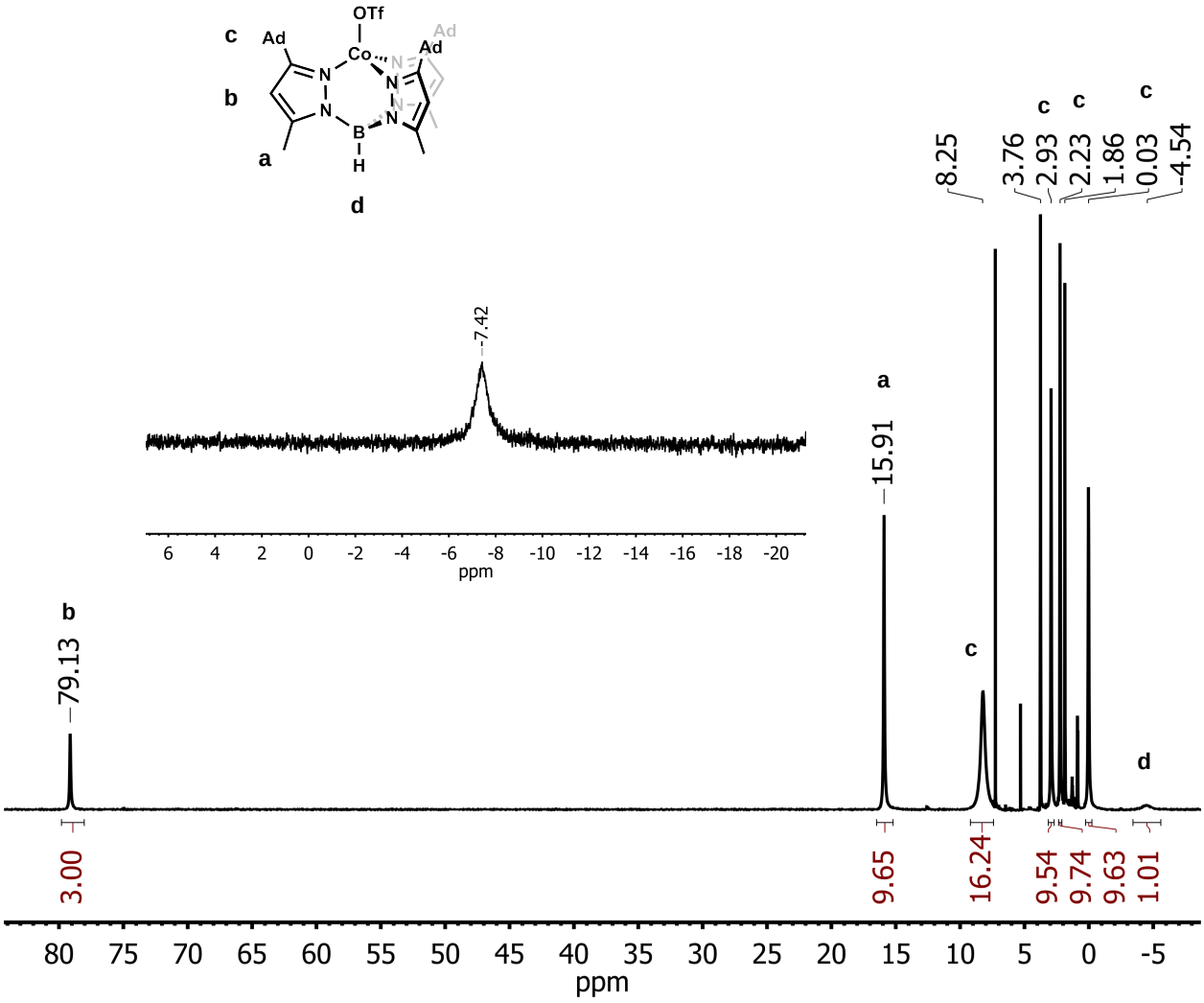

Figure S10. The ^{1}H NMR spectrum of **4** in $CDCl_3$. Inset: ^{19}F NMR spectrum of the same solution. Note: Residual solvent resonances not labeled.

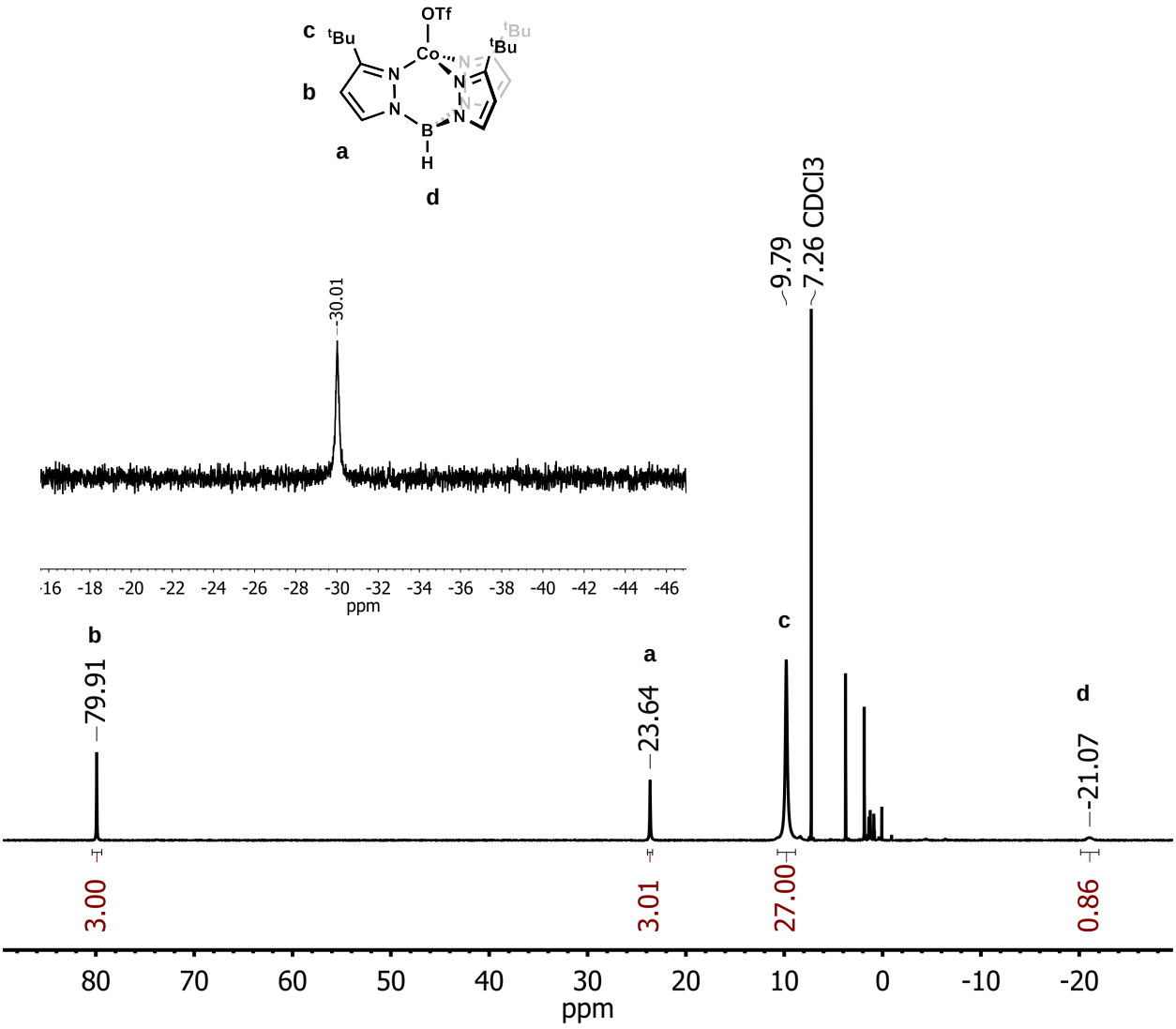

Figure S11. The ^{1}H NMR spectrum of **5** in $CDCl_3$. Inset: ^{19}F NMR spectrum of the same solution. Note: Residual solvent resonances not labeled.

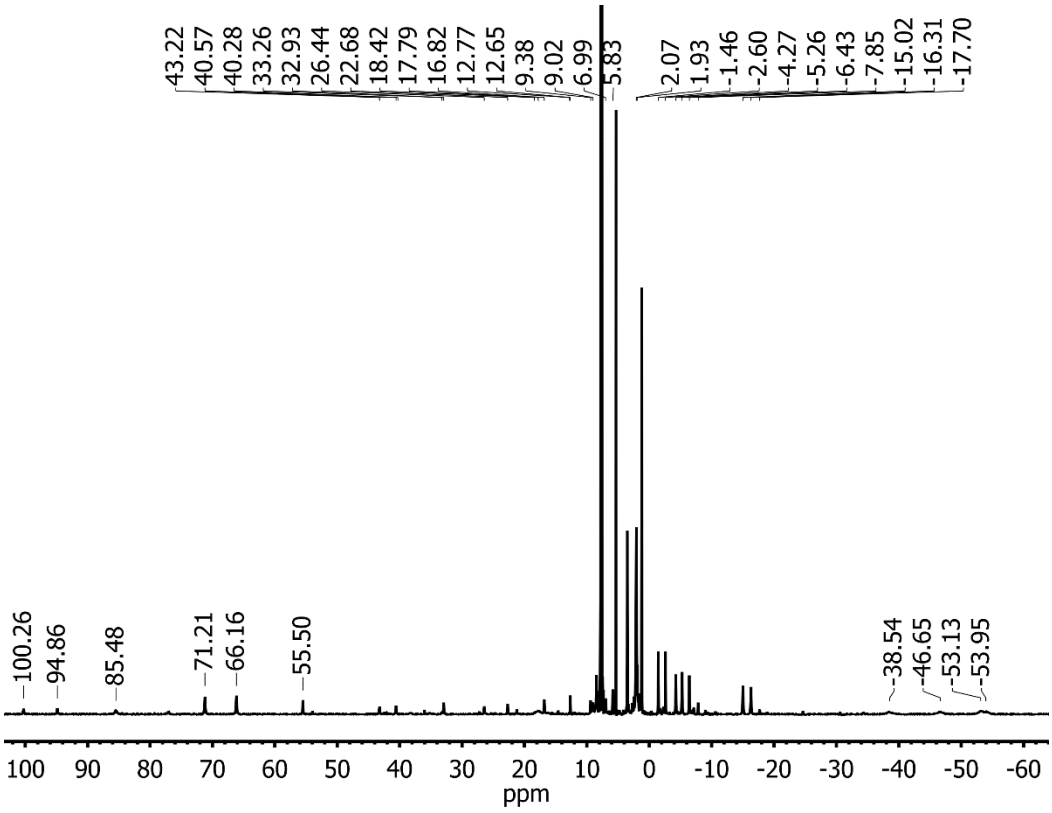

Figure S12. The ^{1}H NMR spectrum of the decay of **1** (2.5 mM in CD_2Cl_2) after 24 h. Note: the top of residual solvent and BAr^F_4 anion peaks have been clipped to better show paramagnetic peaks.

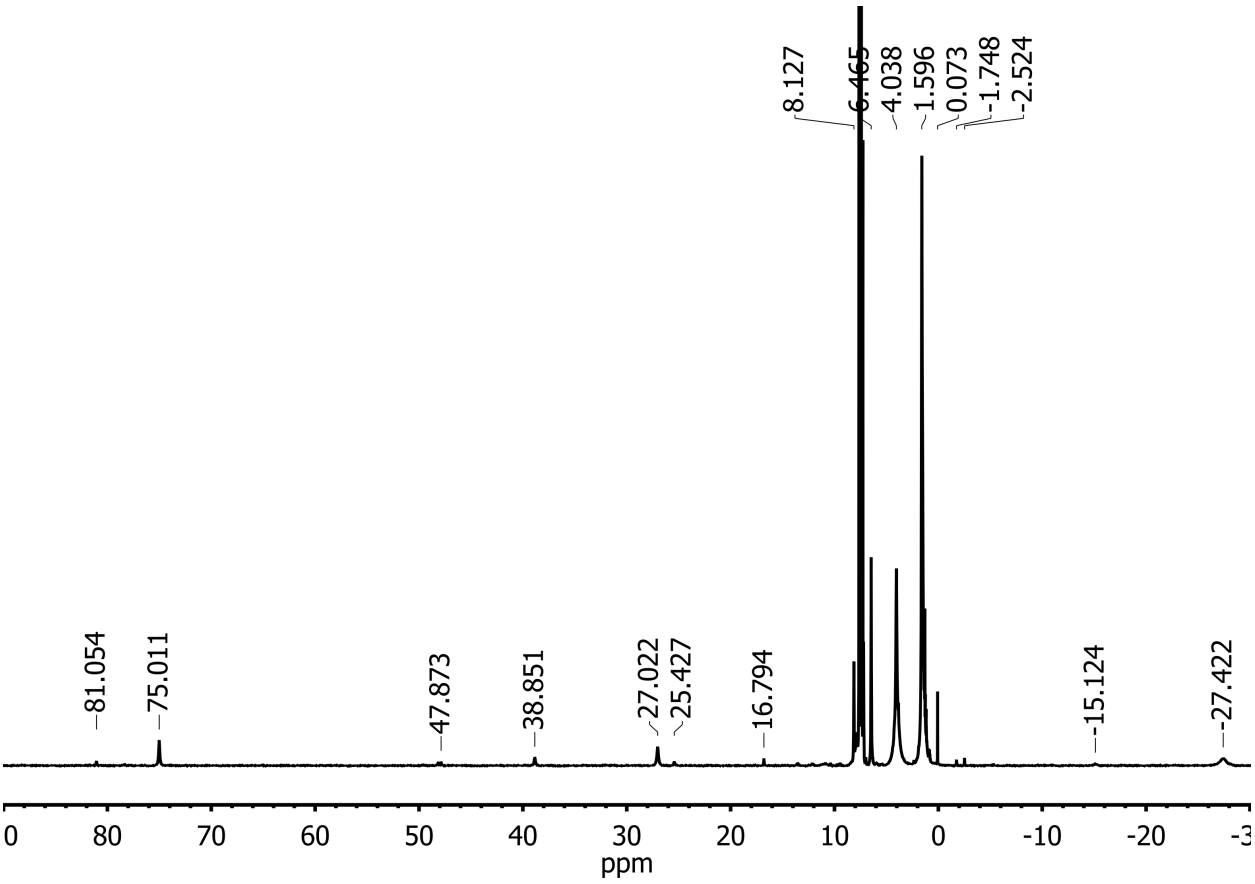

Figure S13. The ^{1}H NMR spectrum of the decay of **2** (in $CDCl_3$) after standing for 14 d in Et_2O. Note: the top of residual solvent and BAr^F_4 anion peaks have been clipped to better show paramagnetic peaks.

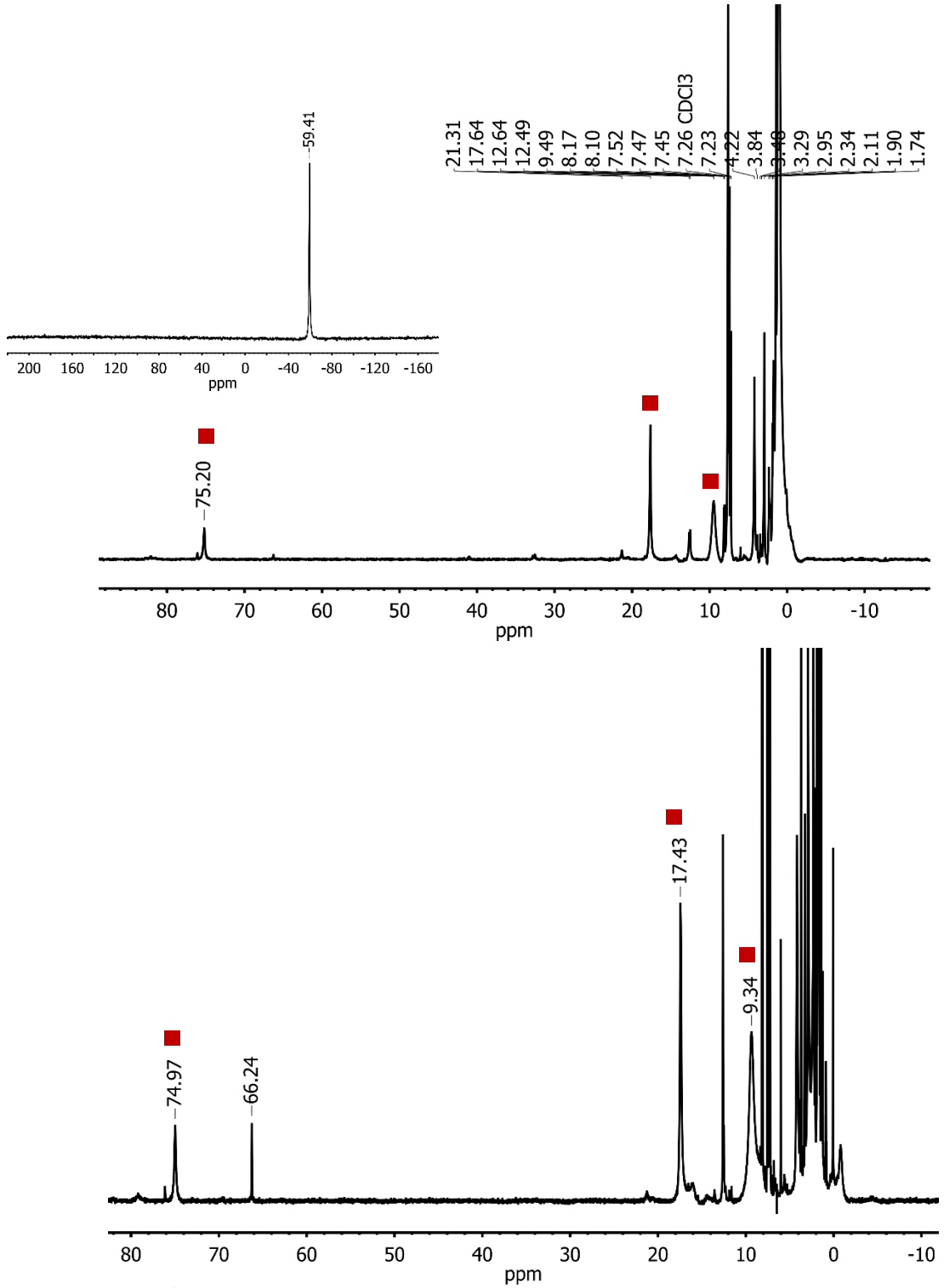

Figure S14. The ^{1}H NMR spectrum of the reaction of **1** (2.5 mM in $CDCl_3$) with (top) 10 equiv of PMe_3 and (bottom) independently prepared $OPMe_3$ ($OPMe_3$ prepared by treating ^{s}PhIO with 1.1 equiv of PMe_3 in $CDCl_3$ and stirring for 1 h). Red squares indicate the putative $OPMe_3$ adduct. Note: the top of the residual solvent peaks and excess PMe_3 have been clipped to better show paramagnetic features. Inset: ^{31}P NMR spectrum of reaction mixture, consistent with free PMe_3.

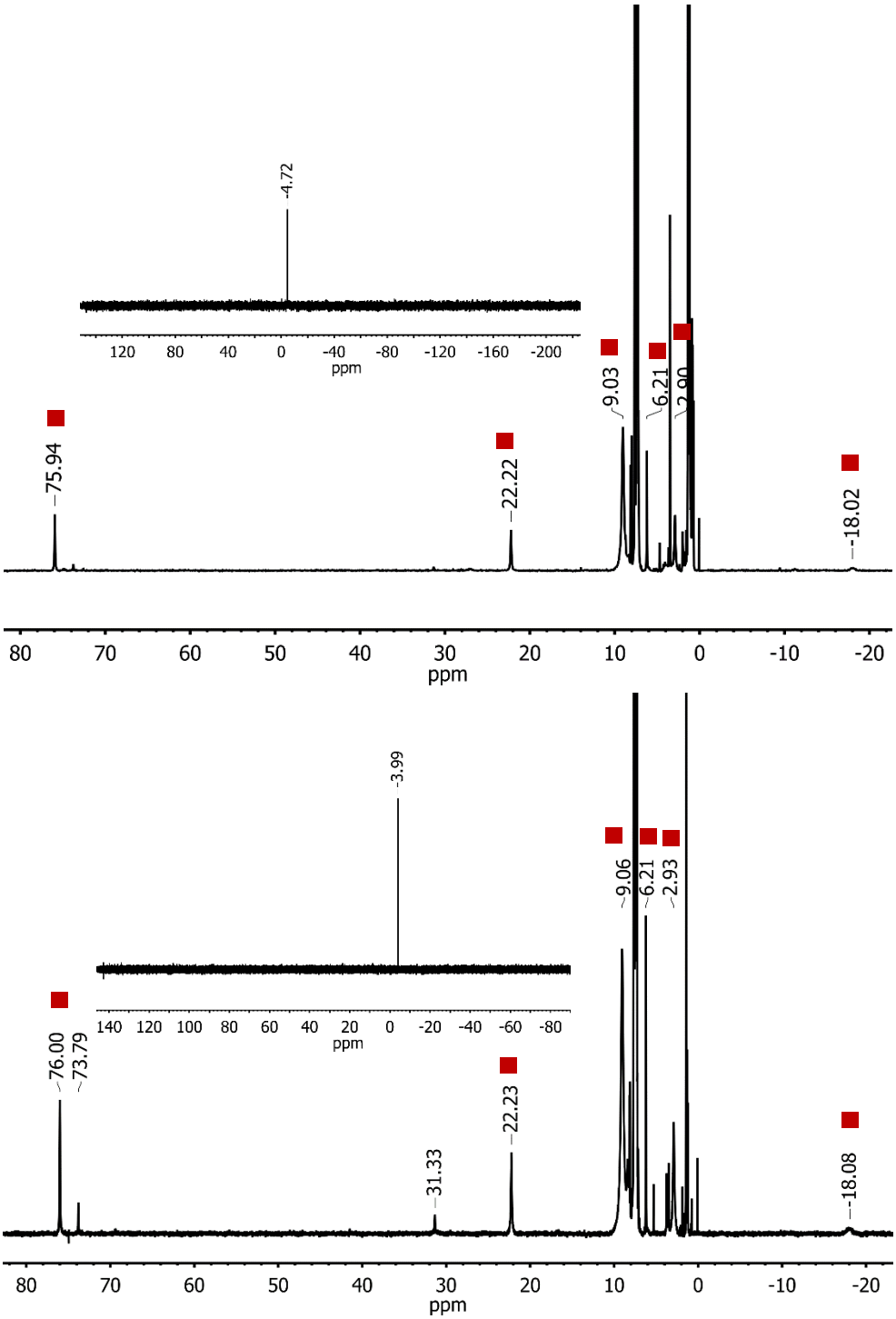

Figure S15. The ^{1}H NMR spectrum ($CDCl_3$) of the 2.5 mM reaction of **2** (top) and **3** (bottom) with 10 equiv of PPh_3. Red squares are assigned to resonances for the $OPPh_3$ adduct, other paramagnetic peaks arise from an unknown impurity. Note: the top of the residual solvent, $BAr^F{}_4$, and excess PPh_3 resonances have been clipped to better show paramagnetic peaks. Inset: ^{31}P NMR spectrum of the respective reaction mixtures consistent with free PPh_3.

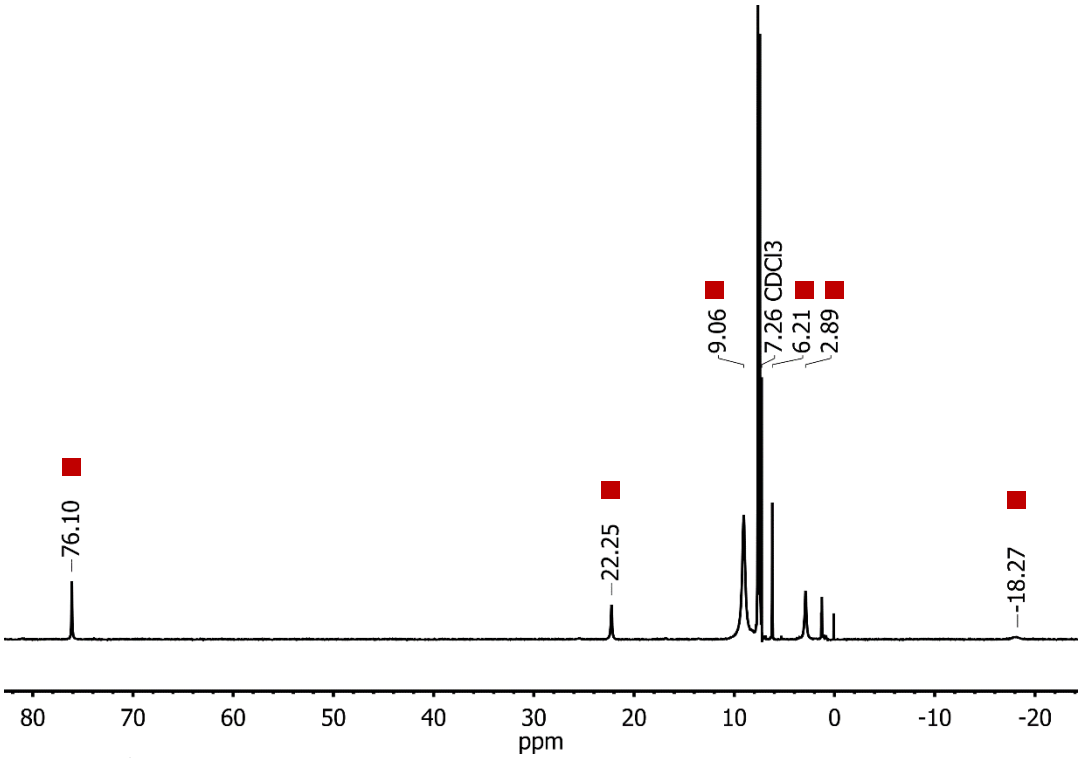

Figure S16: The ^{1}H NMR spectrum of independently synthesized $OPPh_3$ adduct prepared by treatment of a solution of **5** with 1.1 equiv of $OPPh_3$ in the presence of 1.1 equiv $NaBAr^{F}_{4}$. Note: Peaks for residual solvent and BAr^{F}_{4} anion have been clipped off to show detail of paramagnetic features.

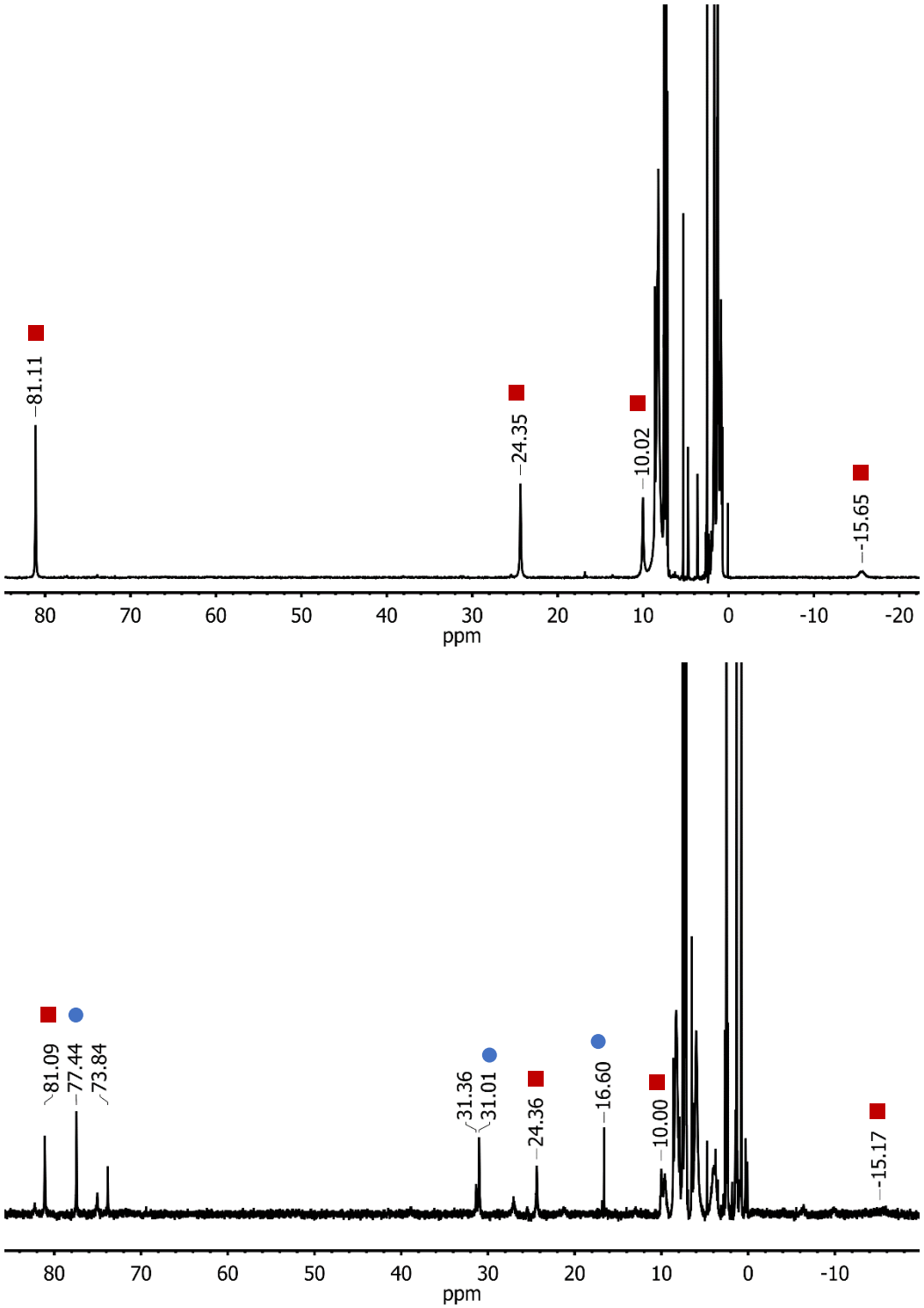

Figure S17. The ^{1}H NMR spectrum of the reaction of **2** (top, $CDCl_3$) and **3** (bottom, 2.5 mM in $CDCl_3$) with 10 equiv thioanisole after 52 and 32 h. Red squares mark resonances for the PhSOMe adduct (see below), blue circles are for **2** formed as the immediate decay product of **3**, and other paramagnetically shifted peaks are from an unknown impurity. Note: The top of the residual solvent peaks and BAr^{F}_{4} resonances have been clipped off to better show paramagnetic features.

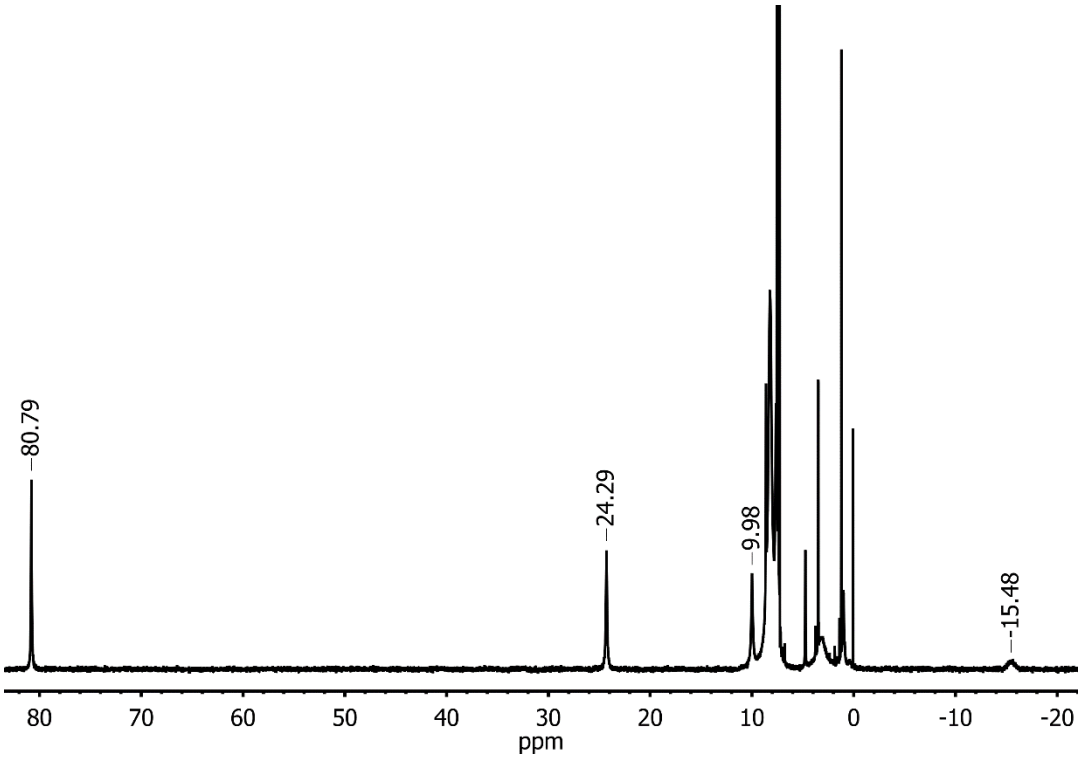

Figure S18. The ^{1}H NMR spectrum of independently prepared CoTp^{tBu}-PhSOMe adduct ($CDCl_3$) generated by the addition of 1.1 equiv of PhSOMe to **2** in the presence of 1.1 equiv $NaBAr^{F}_{4}$. Note: residual solvent peaks have been clipped at the top to better show paramagnetic peaks.

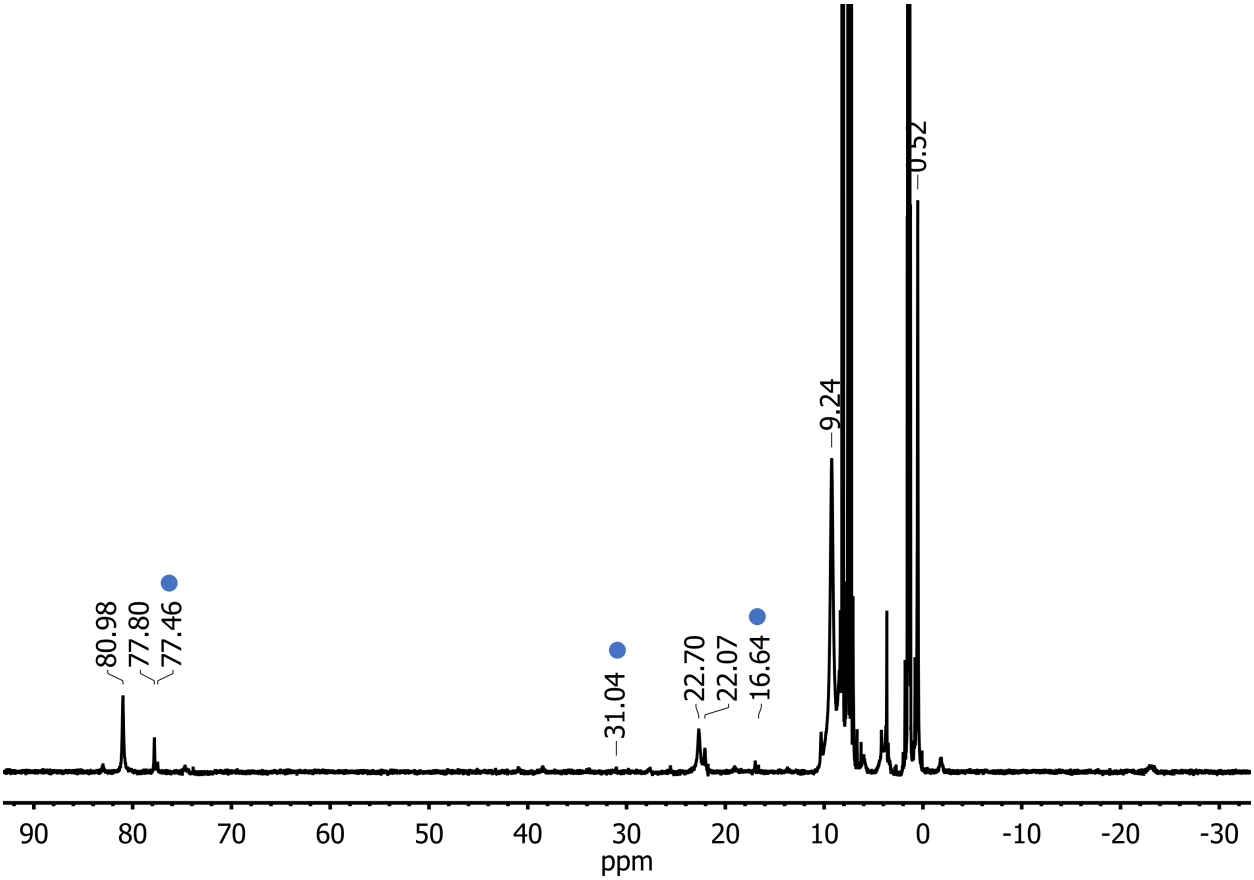

Figure S19. The ^{1}H NMR spectrum of the reaction of **3** with 20 equivalents of ^{s}PhI in $CDCl_3$. Peaks labeled with blue circles correspond to some of complex **2** produced while other labeled resonances belong to unknown paramagnetic products. Note: residual solvent, ^{s}PhI, and BAr^{F}_{4} resonances have been clipped at the top to better show paramagnetic peaks.

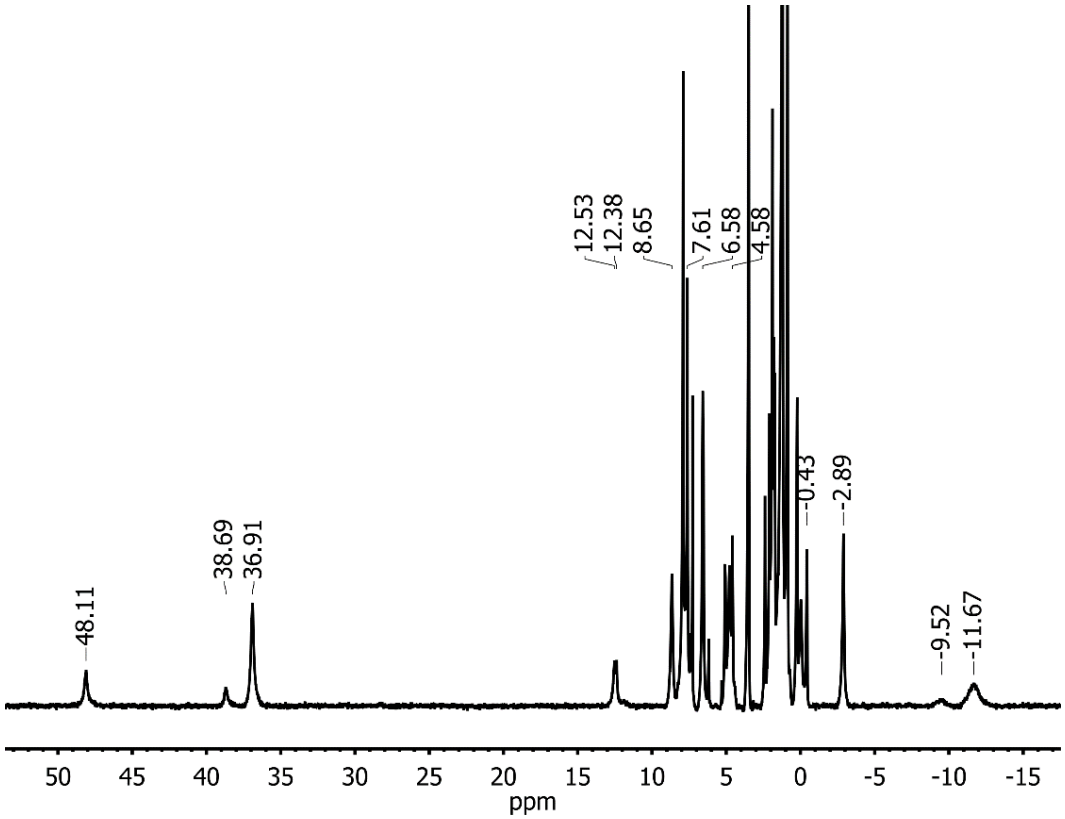

Figure S20. The ^{1}H NMR spectrum of the crystals of **6** obtained from the reaction of **1** with 10 equiv of $ScOTf_3$. Note: the top of residual solvent peaks has been clipped off to better show the paramagnetic features.

2.4 EPR Spectra

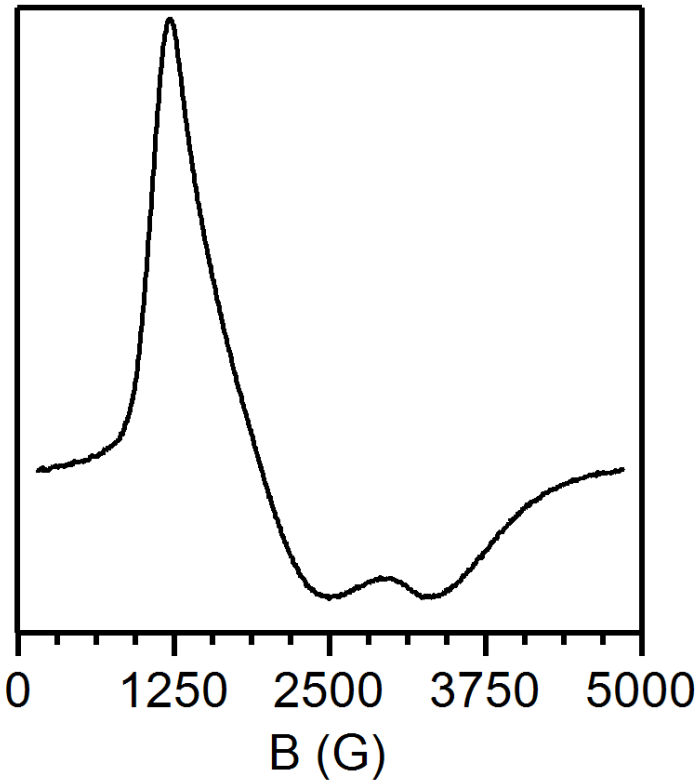

Figure S21. The X-band EPR spectrum of **1** collected on a 15 mM solution in Et_2O at 15 K. Microwave frequency: 9.63 GHz, microwave power: 0.2 mW, and g_{eff} = 5.55, 3.58, and 2.05.

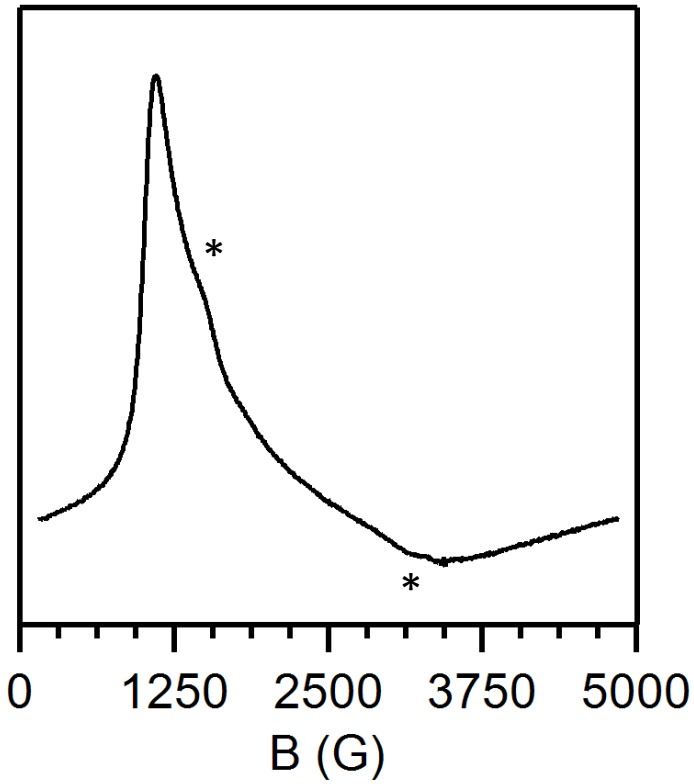

Figure S22. The X-band EPR spectrum of **2** collected on a 15 mM solution in Et_2O at 15 K. Microwave frequency: 9.63 GHz, microwave power: 2.0 mW, and g_{eff} = 6.25, 3.49, and 2.05. Asterisks indicate what is consistent with a small amount of **5**.

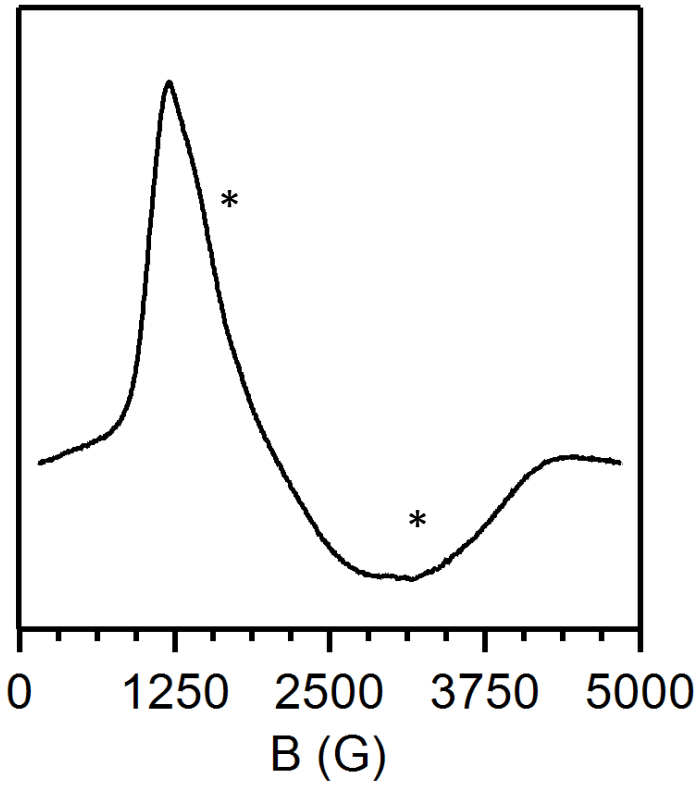

Figure S23. The X-band EPR spectrum of **3** collected on a 15 mM solution in Et_2O at 15 K. Microwave frequency: 9.63 GHz, microwave power: 0.6 mW, and g_{eff} = 5.66, 3.44, and 2.29. Asterisks indicate what is consistent with a small amount of **5**.

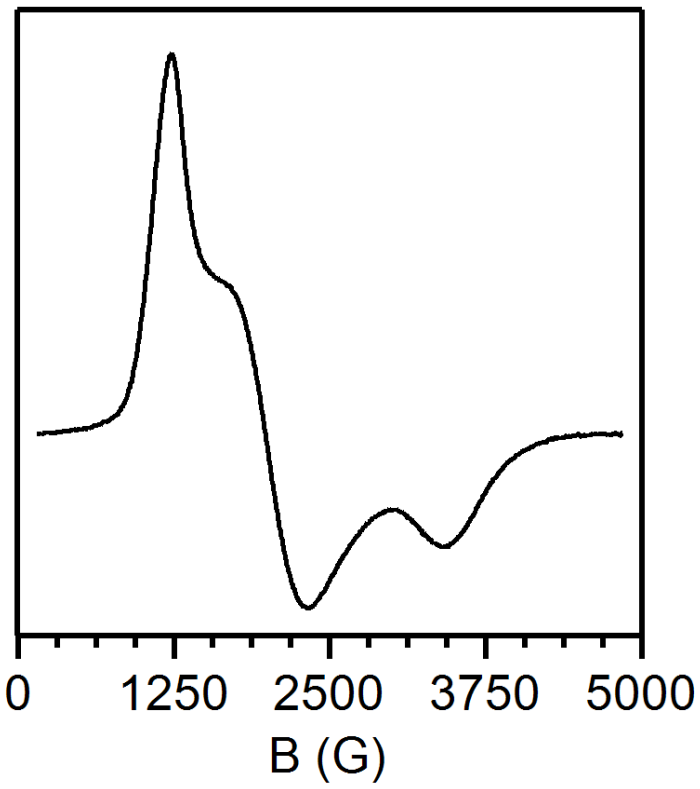

Figure S24. The X-band EPR spectrum of **4** collected on a 15 mM solution in THF at 15 K. Microwave frequency: 9.63 GHz, microwave power: 0.2 mW, and g_{eff} = 5.51, 3.40, and 2.01.

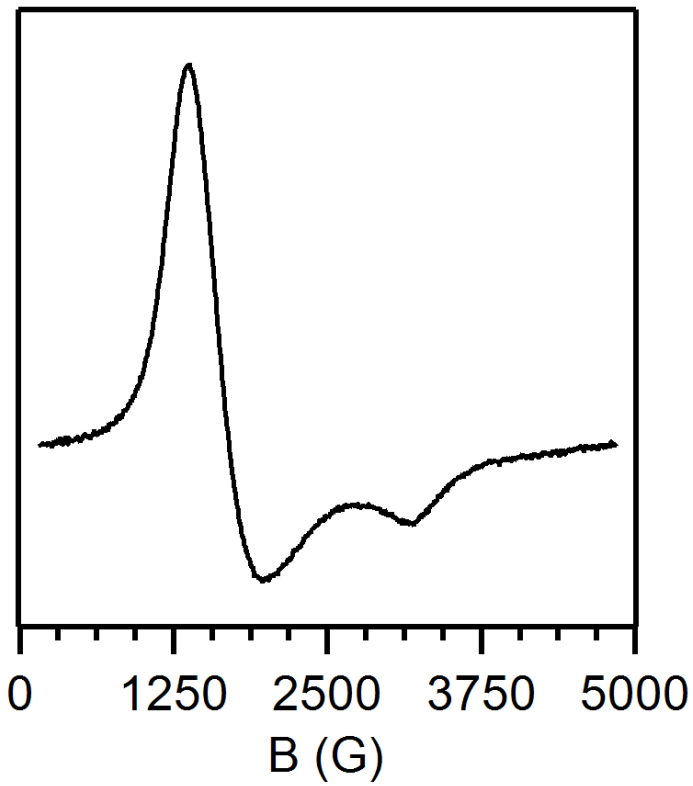

Figure S25. The X-band EPR spectrum of **5** collected on a 15 mM solution in Et_2O at 15 K. Microwave frequency: 9.63 GHz, microwave power: 0.2 mW, and g_{eff} = 5.02, 4.05, and 2.17.

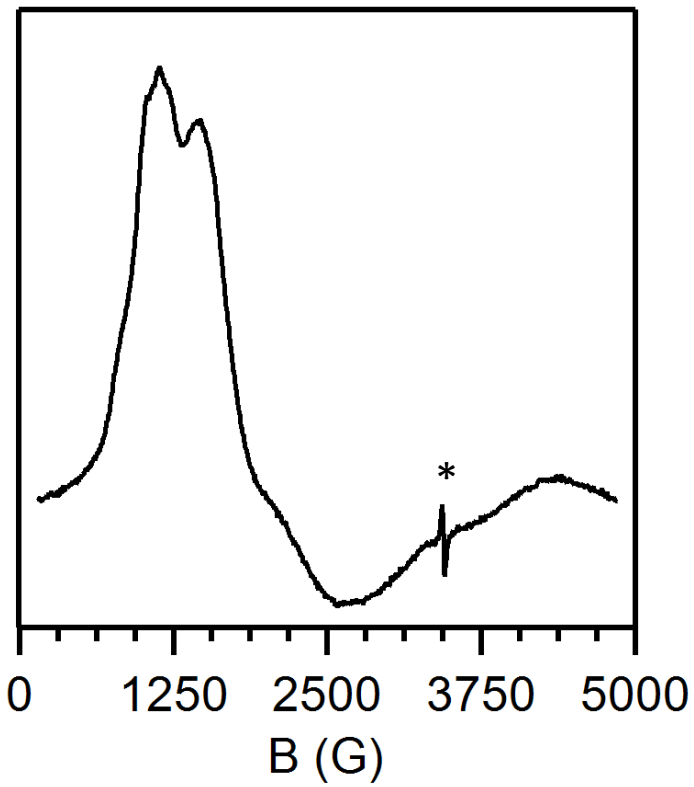

Figure S26. The X-band EPR spectrum of **6** collected on a 9 mM solution in $CDCl_3$ at 15 K. Microwave frequency: 9.63 GHz, microwave power: 4.0 mW, and g_{eff} = 5.66, 3.28, and 2.15. Asterisk indicates an unknown S = ½ impurity.

2.5 Mass Spectra

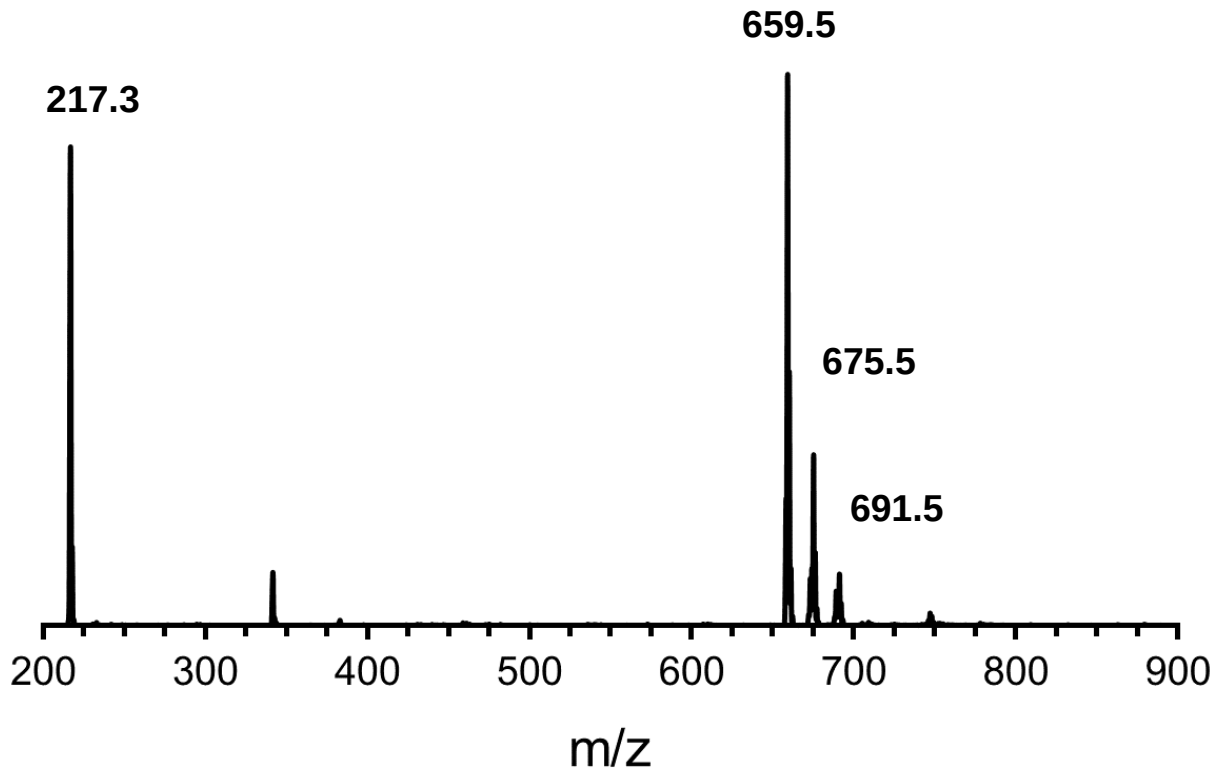

Figure S27. The MS data for the self-decay of **1** (2.5 mM in Et_2O) after 24 h showing free pyrazole (m/z 217.3, $[pz^{Ad,Me}H]^+$), ligand (m/z 659.5, $[H_2Tp^{Ad,Me}]^+$), single oxygen atom incorporation (m/z = 675.5, $[H_2OTp^{Ad,Me}]^+$), and double oxygen atom incorporation (m/z = 691.5 $[H_2O_2Tp^{Ad,Me}]^+$).

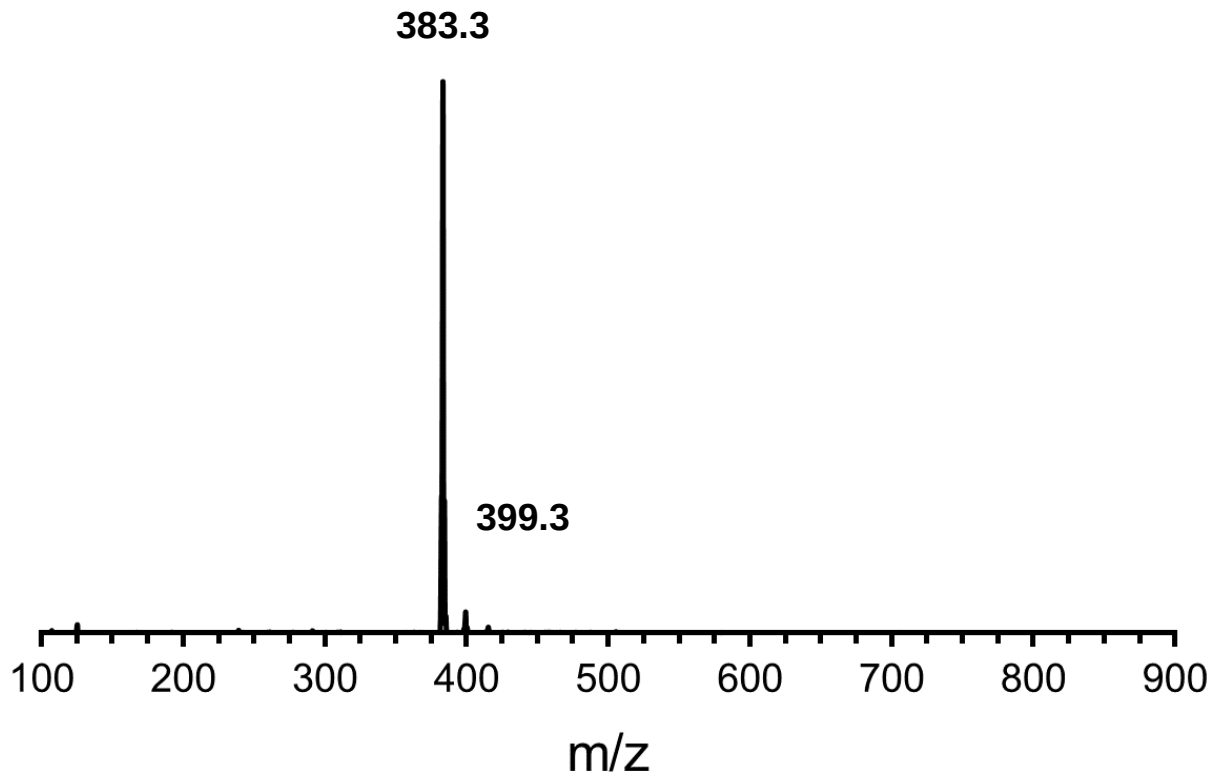

Figure S28. The MS data for the self-decay of **2** (isolated from the decay reaction in Et_2O, after a 1 M HCl_{aq} wash) after 24 h showing free ligand (m/z 383.3, $[H_2Tp^{tBu}]^+$) and single oxygen-atom incorporation (m/z = 399.3, $[H_2OTp^{tBu}]^+$).

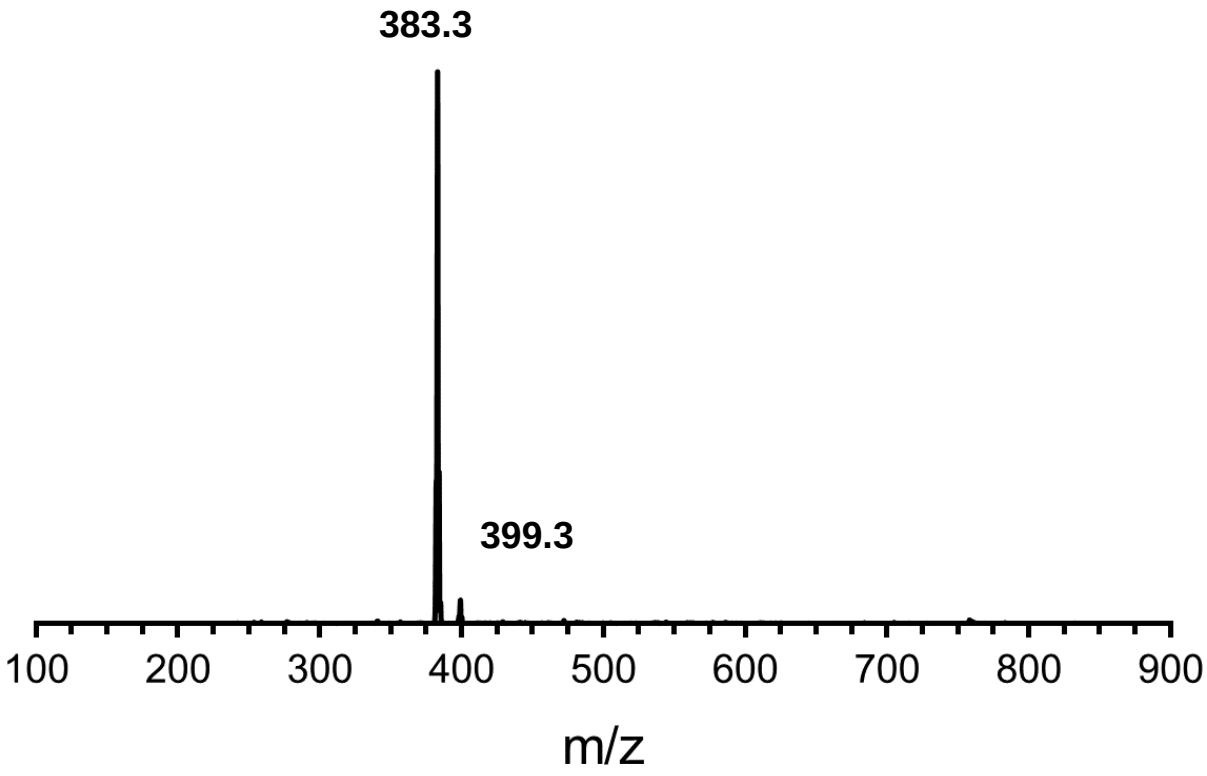

Figure S29. The MS data for the self-decay of **3** (2.5 mM in Et_2O) after 24 h showing free ligand (m/z 383.3, $[H_2Tp^{tBu}]^+$) and single oxygen atom incorporation (m/z = 399.3, $[H_2OTp^{tBu}]^+$).

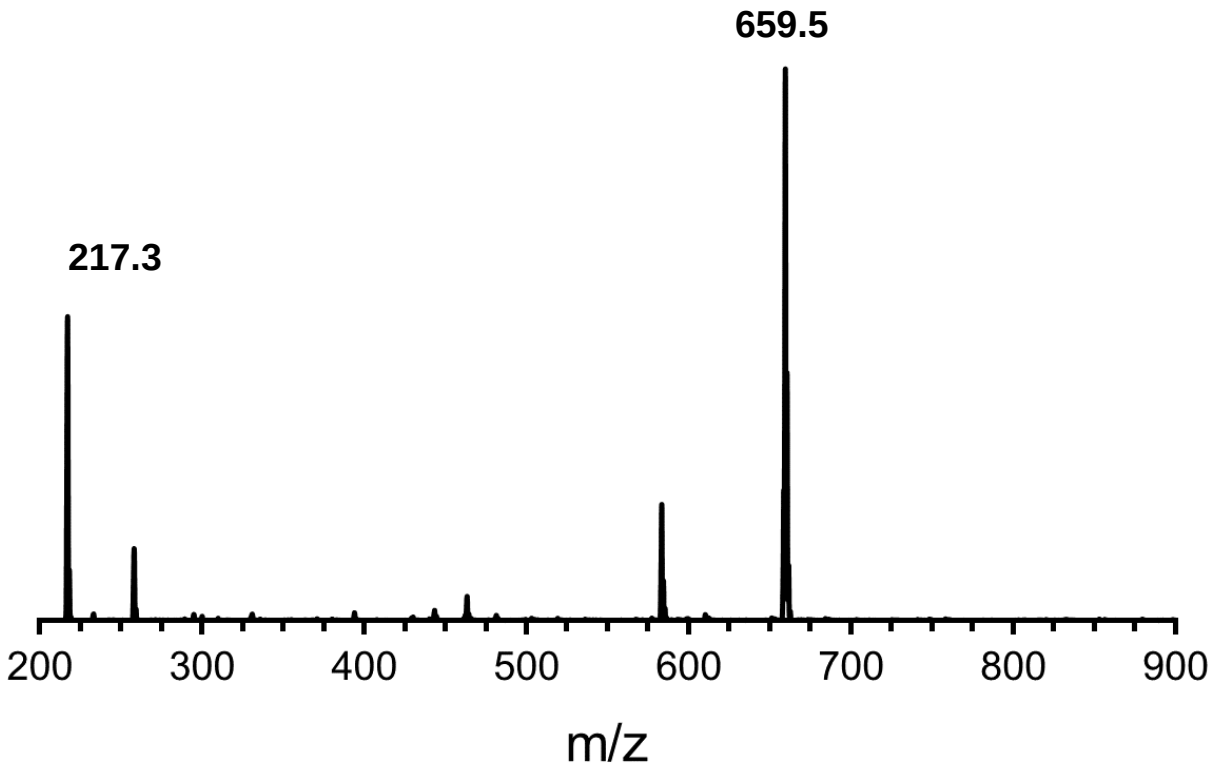

Figure S30. The MS data for the reaction of **1** with 10 equiv of Sc^{3+} ions showing free pyrazole (m/z 217.3 $[pz^{Ad,Me}]^+$) and ligand (m/z = 659.5, $[H_2Tp^{Ad,Me}]^+$).

2.6 Electrochemistry

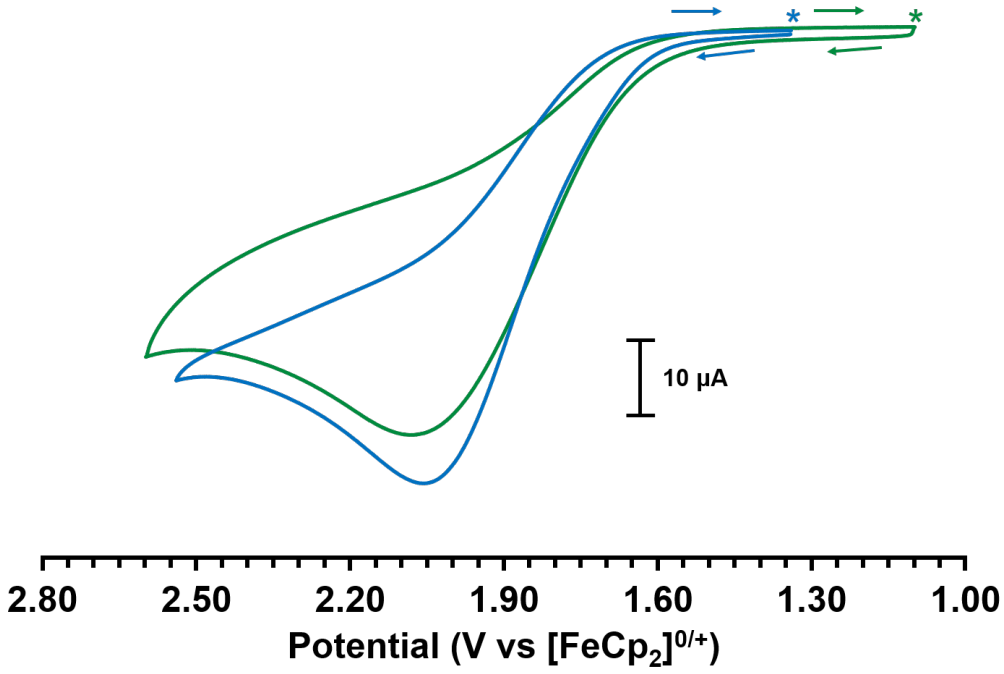

Figure S31. The cyclic voltammograms of **1** (green) and **2** (blue) showing irreversible oxidations at 2.07 and 2.05 V vs. $[FeCp_2]^{0/+}$. Conditions: 5 mM complex with 0.1 M $[Bu_4N][PF_6]$ in DCM, scan rate 100 mV/s, glassy carbon working electrode with platinum wire counter electrode and silver wire as a pseudo-reference. Potentials referenced externally to the $[FeCp_2]^{0/+}$. Asterisks indicate starting potential and arrows indicate direction of sweep.

3.0 Kinetic Experiments

3.1 General Procedure

Data for rate determination were collected in triplicate unless otherwise noted. In a typical experiment, a solution of Co complex was prepared in the appropriate solvent (Et_2O, DCM, or $CDCl_3$). Substrates were then either added as solids, liquids, or concentrated solutions in the same solvent to the Co complex solution to yield a final Co concentration of 2.5 mM. Reaction mixtures were then transferred to either air-free cuvettes fitted with Teflon plugs to be monitored by UV-vis spectroscopy or to J. Young NMR tubes to be monitored by ^{1}H NMR spectroscopy over the course of 24-36 hours. UV-vis spectral data were analyzed by plotting the natural log of the absorbance at a given wavelength at time *t* (A_t) divided by initial absorbance (A_0) vs time in seconds to give the observed rate k_{obs} as the slope of the linear fit of the data. Experiments monitored by ^{1}H NMR spectroscopy were processed and analyzed using the MestReNova software package v 12.0.0-20080 by plotting the integral graph of a given resonance. The data were plotted as the natural log of the integration at time *t* (A_t) divided by initial integration (A_0) vs time in seconds to yield the observed rate k_{obs} as the slope of the linear fit of the data. Plotting the k_{obs} vs concentration of DHA yielded second order rate constants k_2 as the slope of the linear fit of the data.

Kinetic isotope effects (KIEs) were determined using GC-MS data. In a typical experiment, a solution of Co complex (2.5 mM) was prepared using a mixture of 50 equiv each of H_4-DHA and D_4-DHA in a 1:1 molar ratio (for a total of 100 equiv of DHA) dissolved in DCM. The solutions were allowed to stand for 62 hours before being filtered through a column of silica and then subjected to GC-MS analysis. The amount of anthracene present was calculated using a standard calibration curve. Using the relative ratios of the peak intensity at 178.1 and 180.1 m/z for H_2-anthracene and D_2-anthracene, respectively, the concentrations of proteo- and deutero-anthracene were calculated for the starting 1:1 mixture and reaction solutions. After subtracting the quantity of anthracene and d_2-anthracene present in the original mixture from the amount detected in the reaction solutions, the amount of each produced over the course of the reaction could be calculated. The ratio of H_2-anthracene to D_2-anthracene formed during the reaction gave the KIE value. In the case of **1**, ^{s}PhIO, ^{s}PhIO with Sc^{3+}, and ^{s}PhIO with Na^+, the amount of D_2-anthracene produced gave unreasonable values within the error of the measurement. Instead of using the raw data, the standard deviation of the 1:1 mix was used to as a representative amount of D_2-anthracene that may have been produced below a reasonable detection limit. This maximum amount of potential D_2-anthracene provided estimates for the lower bounds of the KIE in these cases. The raw data is provided in **Tables S1** and **S3**, and the substituted data is provided in **Tables S2** and **S4**.

3.2 Kinetic Plots

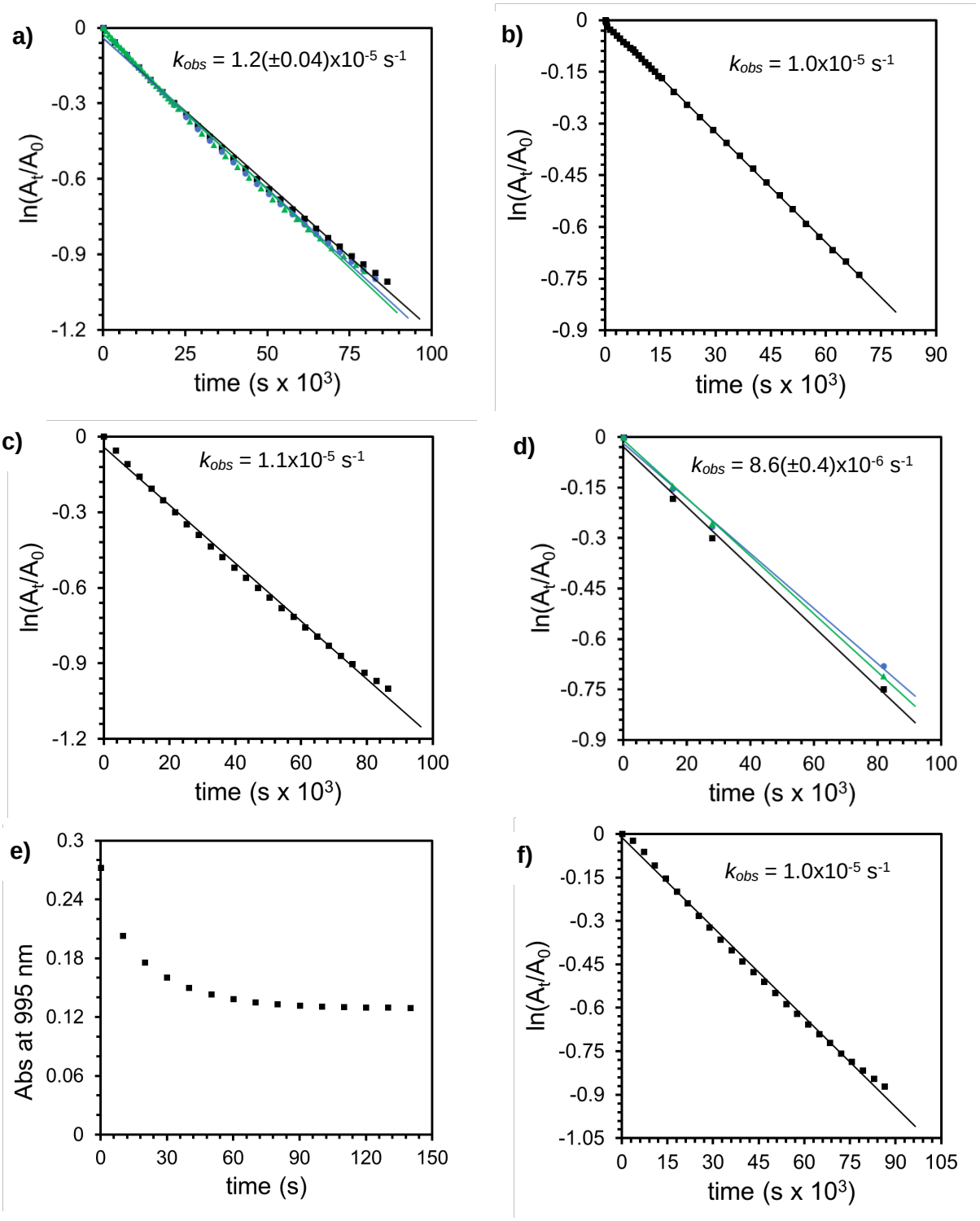

Figure S32. Kinetic data obtained for complex **1** (2.5 mM in Et_2O) a) of the self-decay, b) with 10 equiv of DHA, c) with 10 equiv thioanisole, d) 100 equiv of DHA, e) with 10 equiv PMe_3, and f) with 10 equiv ^{s}PhI. Experiments without errors were not collected in triplicate. Plot for the reaction of **1** with 10 equiv PMe_3 plotted as absorbance vs time as it did not follow pseudo-first order kinetics.

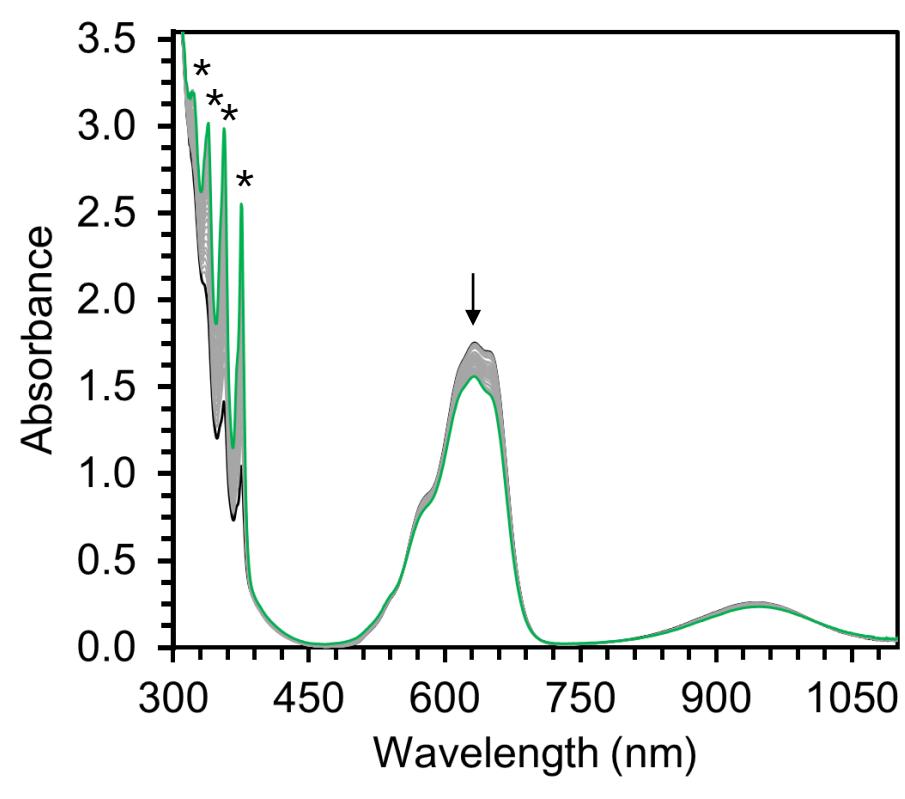

Figure S33. Representative plot of the decay of **2** (2.5 mM in Et_2O) in the presence of 100 equiv of DHA showing both loss of **2** and growth of peaks corresponding to anthracene. Arrow indicates position of wavelength monitored for kinetics, asterisks indicate peaks for anthracene.

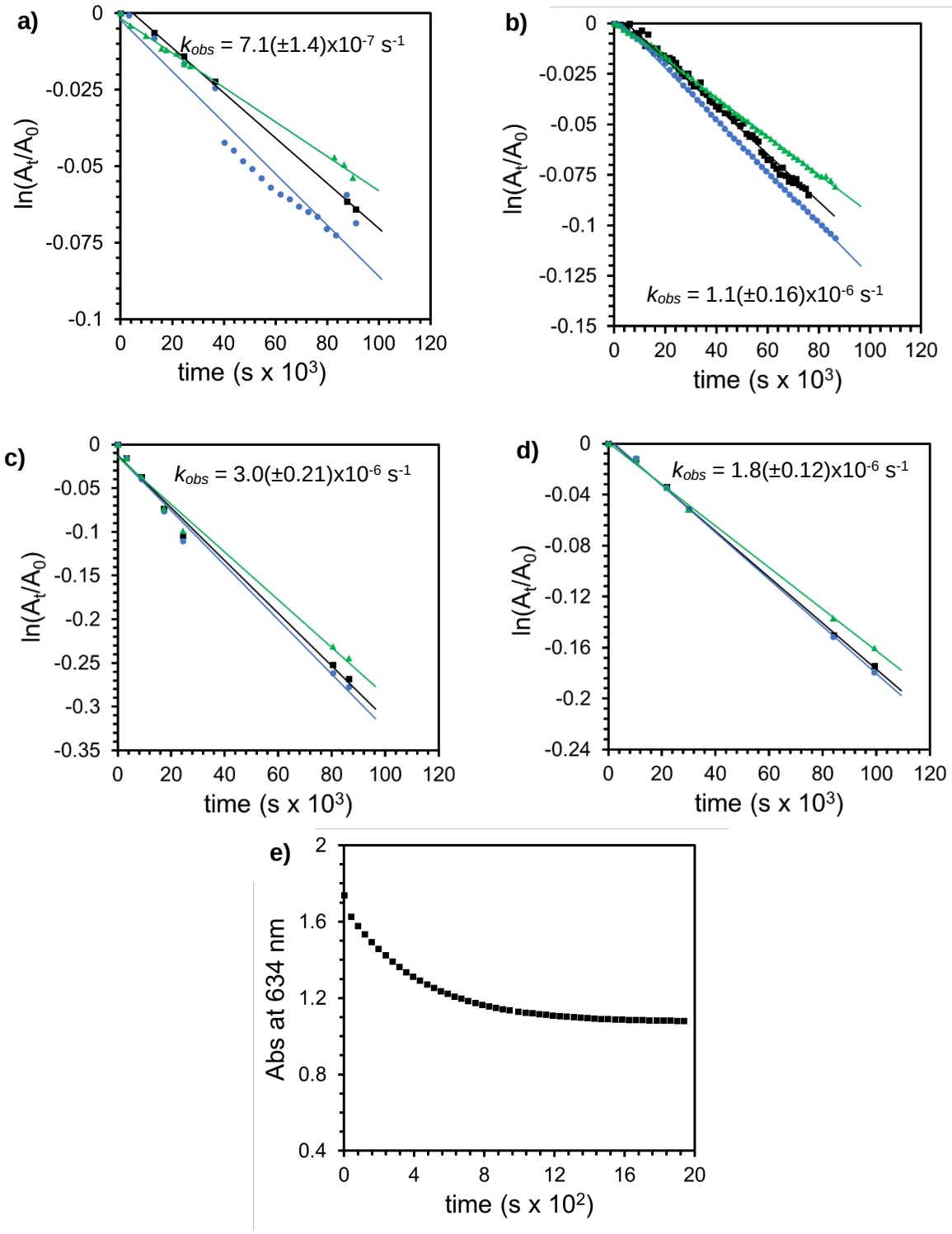

Figure S34. Kinetic data obtained for complex **2** (2.5 mM in Et_2O) a) of the self-decay, b) with 10 equiv of thioanisole, c) with 10 equiv thioanisole and 20 equiv of ^{s}PhI, d) with 20 equiv ^{s}PhI, and e) with 10 equiv PPh_3. Reaction of **2** with 10 equiv PPh_3 plotted as absorbance vs time as it did not follow pseudo-first order kinetics.

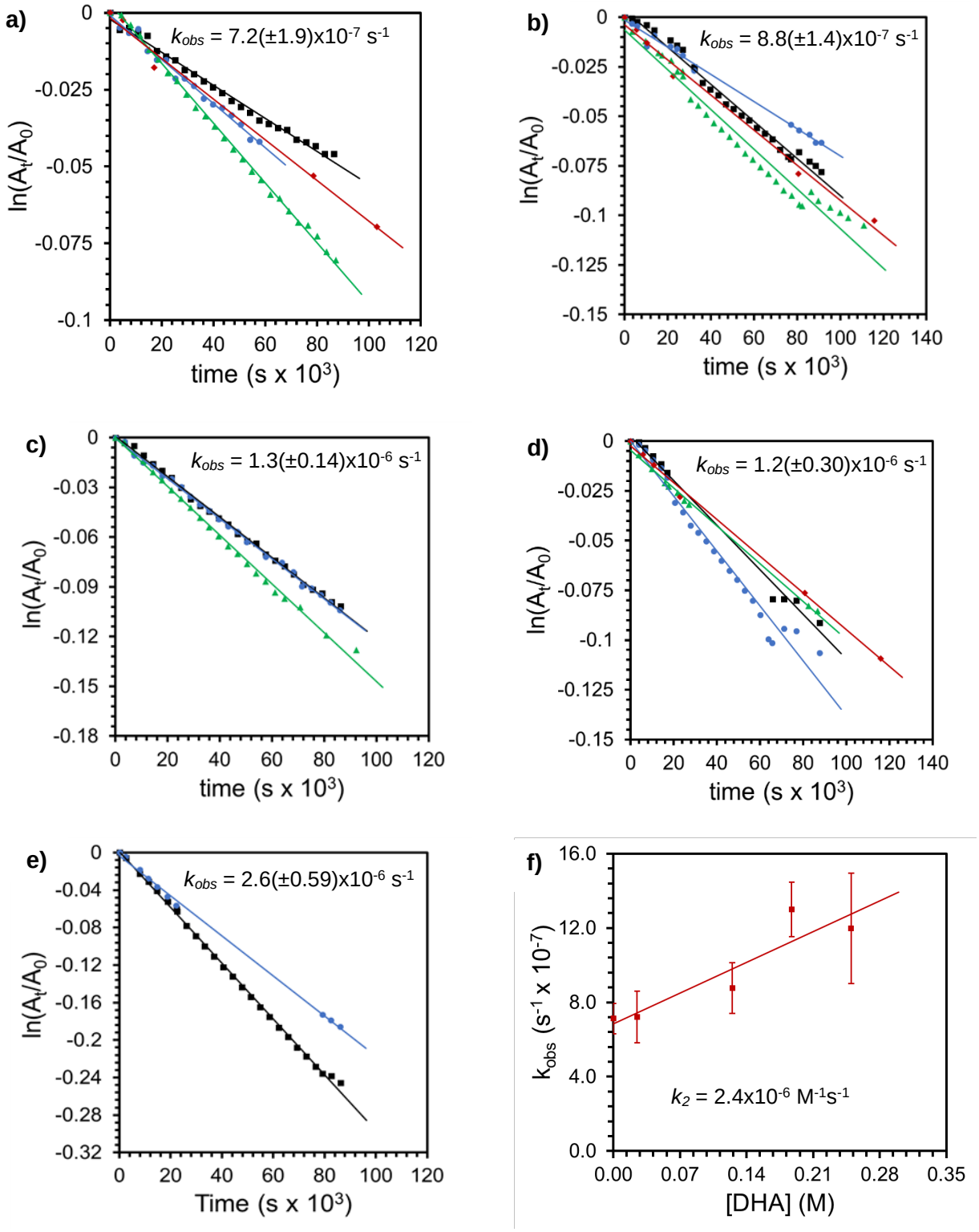

Figure S35. Kinetic data obtained for complex **2** (2.5 mM in Et_2O) a) with 10 equiv DHA, b) with 50 equiv DHA, c) with 75 equiv DHA, d) with 100 equiv of DHA, and e) with 50 equiv DHA and 20 equiv of ^{s}PhI. f) Plot of k_{obs} vs [DHA] to determine the second order rate constant, k_2.

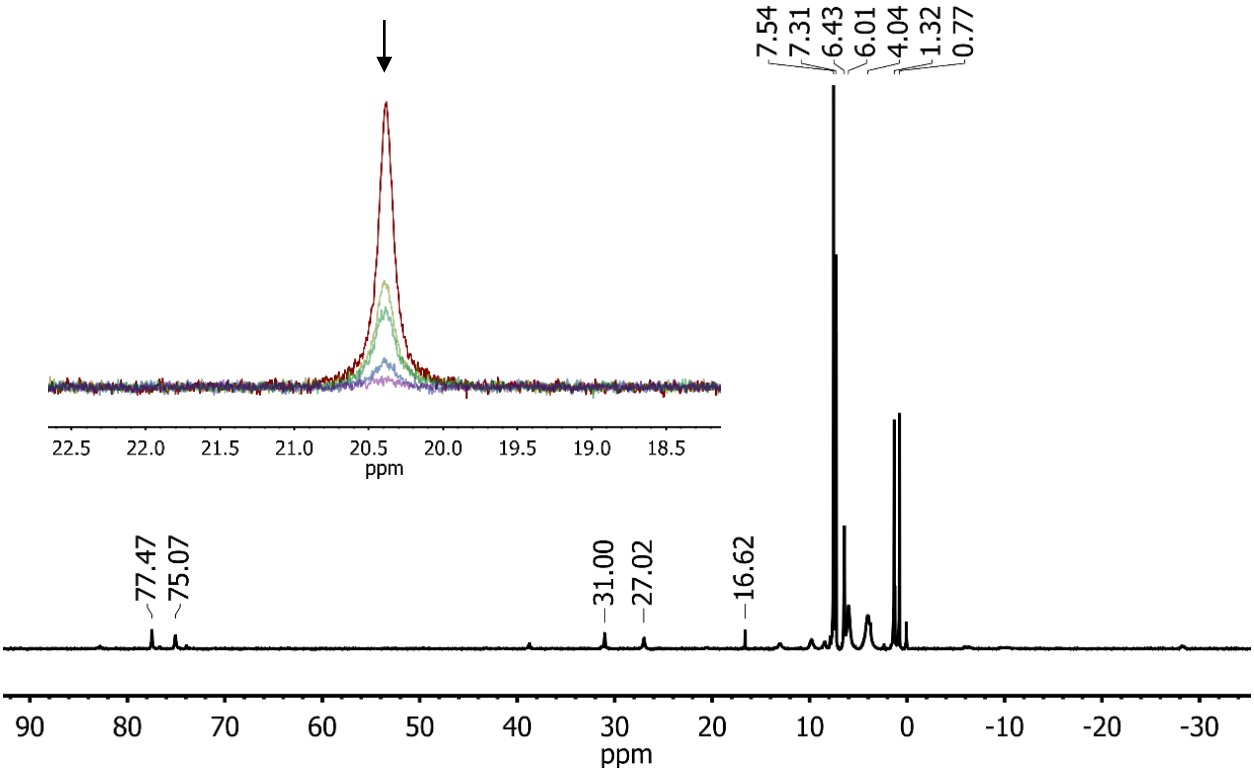

Figure S36. The ^{1}H NMR spectrum of the decay of **3** in $CDCl_3$ after 32 h at room temperature. Inset: overlay of the change in intensity of the 20.4 ppm resonance over time used to calculate k_{obs}.

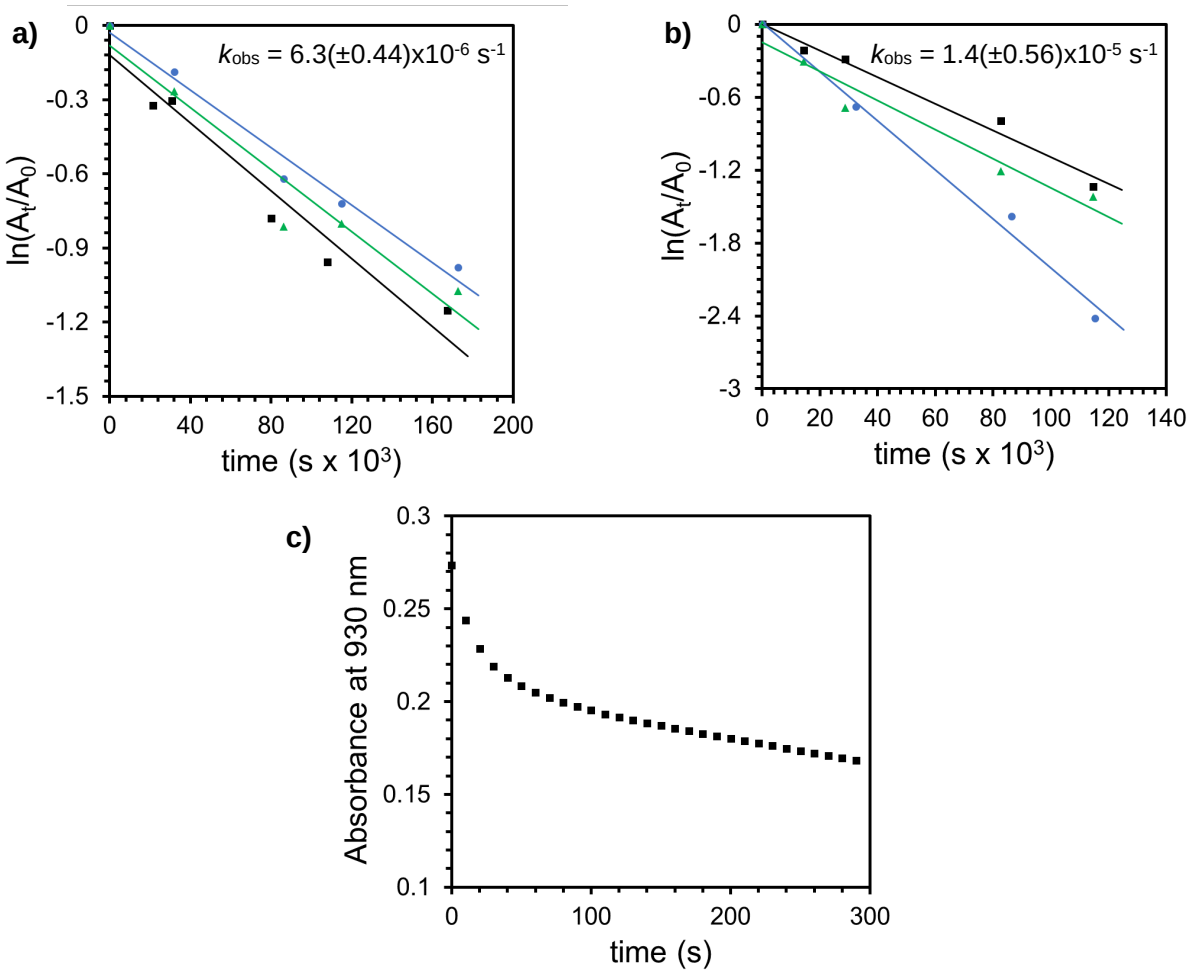

Figure S37. Kinetic data obtained for complex **3** (2.5 mM in $CDCl_3$, monitoring the area of the 20.4 ppm resonance) a) for the self-decay, b) with 10 equiv thioanisole, and c) with 10 equiv PPh_3 (2.5 mM Co complex in Et_2O). Plot of the reaction of **3** with 10 equiv PPh_3 shown as absorbance vs time as it did not fit pseudo-first order kinetics.

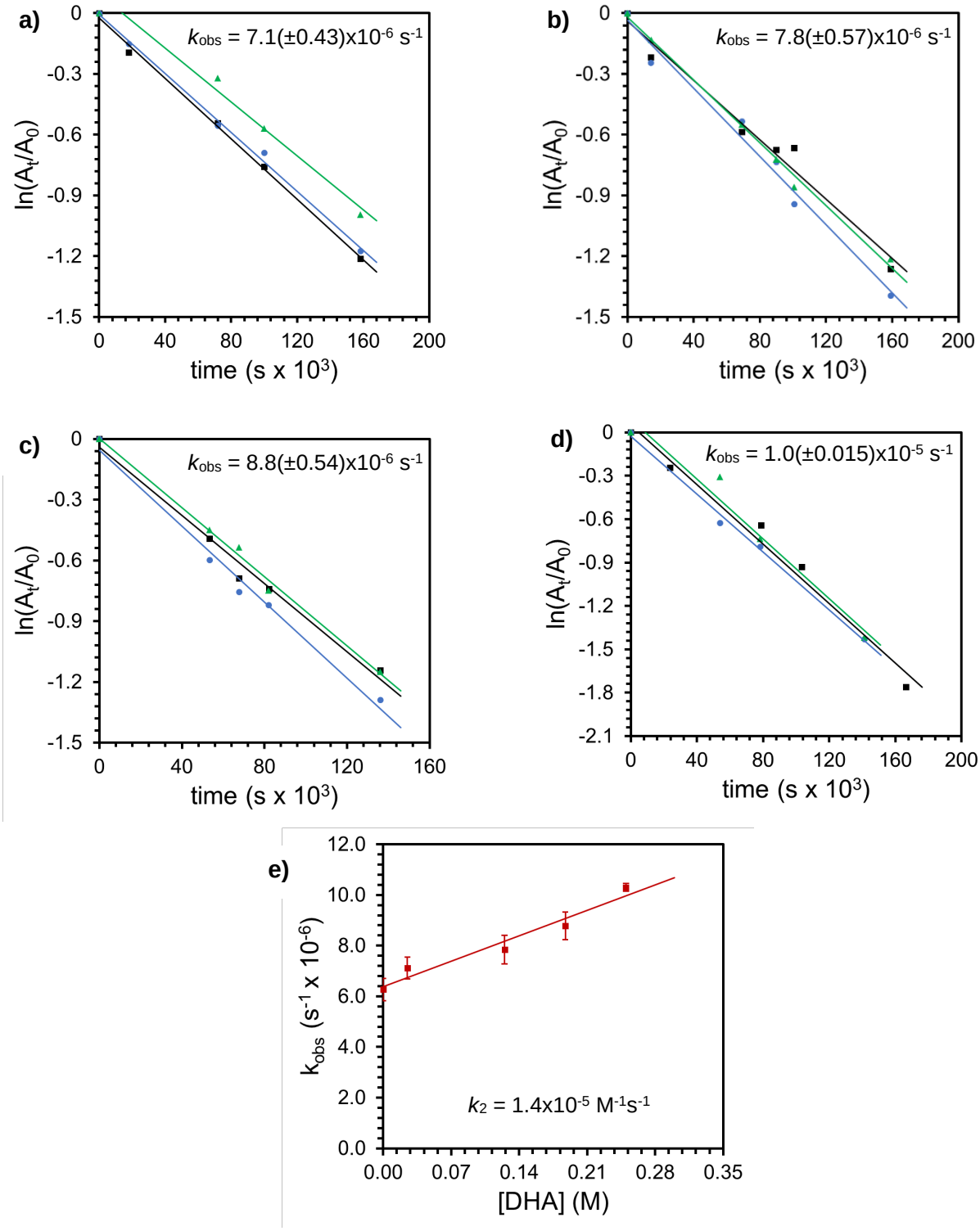

Figure S38. Kinetic data obtained for complex **3** (2.5 mM in $CDCl_3$, monitoring the area of the 20.4 ppm resonance) a) with 10 equiv DHA, b) with 50 equiv DHA, c) with 75 equiv DHA, and d) with 100 equiv of DHA and e) plot of k_{obs} vs [DHA] to determine the second order rate constant, k_2.

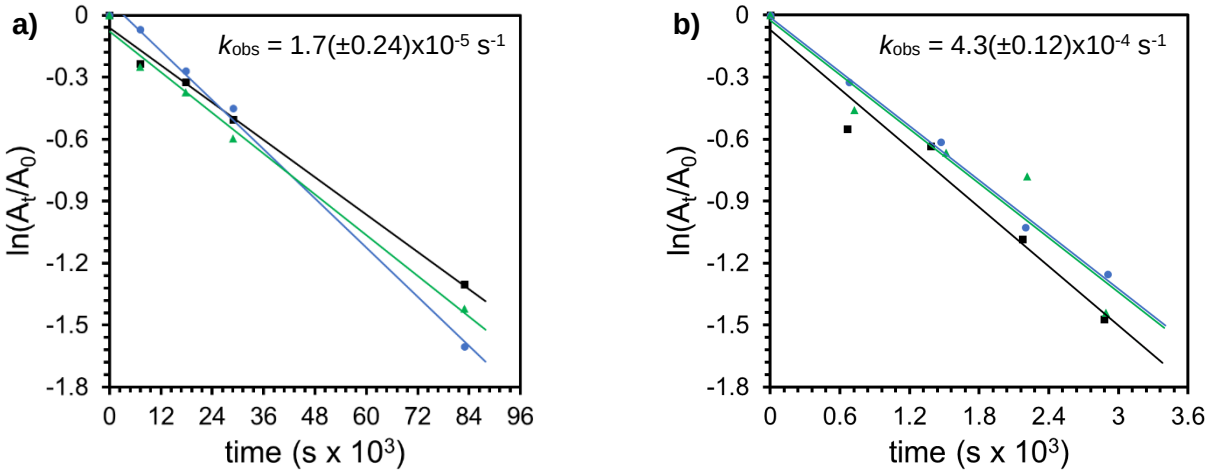

Figure S39. Kinetic data obtained for the background reaction of ^{s}PhIO (2.5 mM in $CDCl_3$, monitoring the area of the 8.0 ppm resonance for loss of ^{s}PhIO) a) with 50 equiv DHA and b) with 10 equiv thioanisole.

3.3 Kinetic Isotope Effects

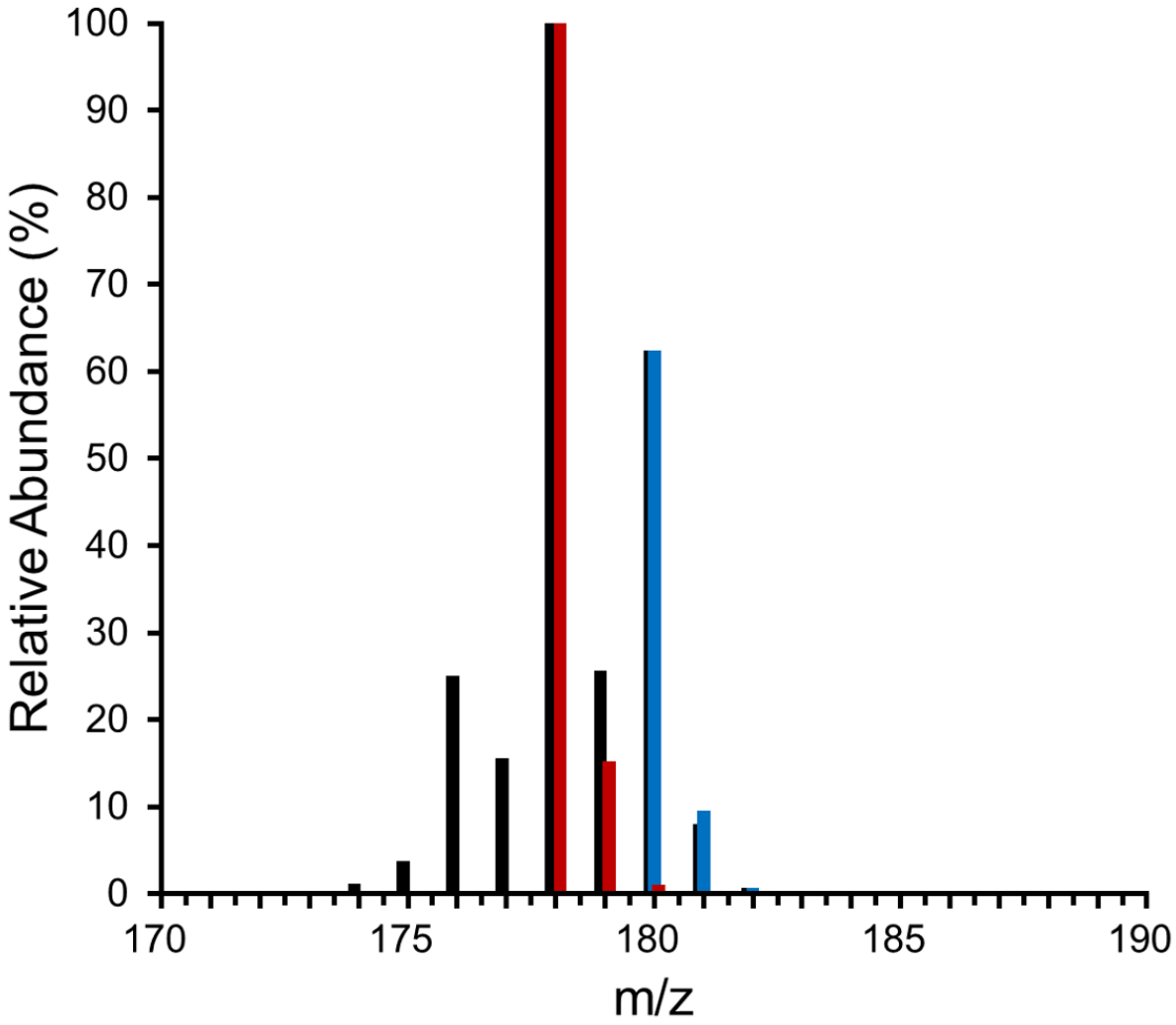

Figure S40. A representative MS trace for determination of the KIE from the reaction of **1** with a 1:1 molar ratio of H_4-DHA:D_4-DHA in DCM at 25 °C. Black bars are experimental data, red bars are isotope modeling of anthracene, and blue bars are isotope modeling of D_2-anthracene.

sample	Total [anthracene] mM	[anthracene] detected mM		[anthracene] Increase mM		KIE	average KIE
1:1 mix		proteo	deutero	proteo	deutero		
trial 1	0.0087	0.0024	0.0063	N/A	N/A		
trial 2	0.0100	0.0027	0.0073	N/A	N/A		
trial 3	0.0103	0.0029	0.0074	N/A	N/A		
1							
Trial 1	0.0152	0.0094	0.0059	0.0069	-0.0004	-	
Trial 2	0.0164	0.0100	0.0064	0.0074	-0.0009	-	
Trial 3	0.0160	0.0098	0.0062	0.0069	-0.0012	-	-
2							
Trial 1	0.0259	0.0188	0.0071	0.0164	0.0008	20.0	
Trial 2	0.0318	0.0231	0.0088	0.0204	0.0015	13.7	
Trial 3	0.0365	0.0266	0.0099	0.0237	0.0025	9.5	14(±5)
3							
Trial 1	0.0253	0.0174	0.0079	0.0150	0.0016	9.4	
Trial 2	0.0304	0.0213	0.0091	0.0187	0.0018	10.3	
Trial 3	0.0332	0.0231	0.0100	0.0203	0.0026	7.8	9(±1)
^{s}PhIO							
Trial 1	0.0107	0.0042	0.0066	0.0017	0.0003	5.8	
Trial 2	0.0119	0.0046	0.0073	0.0019	0.0000	-	
Trial 3	0.0122	0.0048	0.0075	0.0019	0.0000	-	-

Table S1: Raw data and KIE values determined for the reactions of **1**, **2**, **3**, and ^{s}PhIO with a 250 mM 1:1 mixture of H_4-DHA:D_4-DHA in DCM.

sample	Total [anthracene] mM	[anthracene] mM		[anthracene] Increase mM		KIE	average KIE
1:1 mix		proteo	deutero	proteo	deutero		
trial 1	0.0087	0.0024	0.0063	N/A	N/A		
trial 2	0.0100	0.0027	0.0073	N/A	N/A		
trial 3	0.0103	0.0029	0.0074	N/A	N/A		
1							
Trial 1	0.0152	0.0094	0.0059	0.0069	0.0006	>11.6	
Trial 2	0.0164	0.0100	0.0064	0.0074	0.0006	>12.3	
Trial 3	0.0160	0.0098	0.0062	0.0069	0.0006	>11.5	>12
2							
Trial 1	0.0259	0.0188	0.0071	0.0164	0.0008	20.0	
Trial 2	0.0318	0.0231	0.0088	0.0204	0.0015	13.7	
Trial 3	0.0365	0.0266	0.0099	0.0237	0.0025	9.5	14(±5)
3							
Trial 1	0.0253	0.0174	0.0079	0.0150	0.0016	9.4	
Trial 2	0.0304	0.0213	0.0091	0.0187	0.0018	10.3	
Trial 3	0.0332	0.0231	0.0100	0.0203	0.0026	7.8	9(±1)
^{s}PhIO							
Trial 1	0.0107	0.0042	0.0066	0.0017	0.0006	>2.9	
Trial 2	0.0119	0.0046	0.0073	0.0019	0.0006	>3.2	
Trial 3	0.0122	0.0048	0.0075	0.0019	0.0006	>3.2	>3

Table S2: KIE values determined for the reactions of **1**, **2**, **3**, and ^{s}PhIO with DHA using a minimum detectable value to replace increases in D_2-anthracene that are smaller than the standard deviation from the 1:1 mix. The average concentration of D_2-anthracene in the 1:1 mix is 0.007(±0.0006) mM. Shown in red are cases where the standard deviation of 0.0006 mM was used as the maximum amount of D_2-anthracene that could be produced but not measured above error. Using this maximum value provides a lower bound for the KIE.

sample	Total [anthracene] mM	[anthracene] mM		[anthracene] Increase mM		KIE	average KIE
1:1 mix		proteo	deutero	proteo	deutero		
trial 1	0.0385	0.0150	0.0236	N/A	N/A		
trial 2	0.0376	0.0140	0.0236	N/A	N/A		
trial 3	0.0415	0.0154	0.0260	N/A	N/A		
^{s}PhIO + Sc^{3+}							
Trial 1	0.142	0.120	.0215	0.106	-0.0021	-	
Trial 2	0.111	0.0942	0.0170	0.0802	-0.0065	-	
Trail 3	0.136	0.115	0.0206	0.0999	-0.0055	-	-
^{s}PhIO + Na^{+}							
Trial 1	0.0505	0.0310	0.0195	0.0160	-0.0041	-	
Trial 2	0.0458	0.0282	0.0175	0.0142	-0.0060	-	
Trial 3	0.0506	0.0313	0.0193	0.0159	-0.0068	-	-

Table S3: Raw GCMS data for the reactions of ^{s}PhIO in the presence of Lewis acids with DHA for KIE calculations. Conditions: 2.5 mM ^{s}PhIO, 2.5 mM Lewis acid, and 250 mM of 1:1 H_4-DHA:D_4-DHA mixture in DCM, left to stir for 65 h at room temperature.

sample	Total [anthracene] mM	[anthracene] mM		[anthracene] Increase mM		KIE	average KIE
1:1 mix		proteo	deutero	proteo	deutero		
trial 1	0.0385	0.0150	0.0236	N/A	N/A		
trial 2	0.0376	0.0140	0.0236	N/A	N/A		
trial 3	0.0415	0.0154	0.0260	N/A	N/A		
^{s}PhIO + Sc^{3+}							
Trial 1	0.142	0.120	.0215	0.106	0.0014	74	
Trial 2	0.111	0.0942	0.0170	0.0802	0.0014	56	
Trail 3	0.136	0.115	0.0206	0.0999	0.0014	70	>66
^{s}PhIO + Na^{+}							
Trial 1	0.0505	0.0310	0.0195	0.0160	0.0014	11	
Trial 2	0.0458	0.0282	0.0175	0.0142	0.0014	10	
Trial 3	0.0506	0.0313	0.0193	0.0159	0.0014	11	>11

Table S4: KIE values determined for the reactions of ^{s}PhIO with DHA in the presence of Lewis acids using a minimum detectable value to replace increases in D_2-anthracene that are smaller than the standard deviation from the 1:1 mix. The average concentration of D_2-anthracene in the 1:1 mix is 0.024(±0.0014) mM. Shown in red are cases where the standard deviation of 0.0014 mM was used as the maximum amount of D_2-anthracene that could be produced but not measured above error. Using this maximum value provides a lower bound for the KIE.

4.0 X-ray Crystallography

4.1 General Descriptions

The diffraction data for **3** were measured at 100 K on a Bruker D8 fixed-chi with PILATUS1M (CdTe) pixel array detector (synchrotron radiation, λ = 0.41328 Å (30 KeV)) at the Chem-MatCARS 15-ID-B beamline at the Advanced Photon Source (Argonne National Laboratory). The diffraction data for **1**, **2**, **4**, **5**, and **6** were measured at 100 K on a Bruker D8 VENTURE diffractometer equipped with a microfocus Mo-target X-ray tube (λ = 0.71073 Å) and PHOTON 100 CMOS detector. Data reduction and integration were performed with the Bruker APEX3 software package (Bruker AXS, version 2017.3-0, 2018). Data were scaled and corrected for absorption effects using the multi-scan procedure as implemented in SADABS (Bruker AXS, version 2014/5).[8] The structures was solved by SHELXT (Version 2014/5)[9] and refined by a full-matrix least-squares procedure using OLEX2 (XL refinement program version 2018/1).[10,11] Crystallographic data and details of the data collection and structure refinement are listed in Section 4.4 of this supplementary information.

4.2 Structures

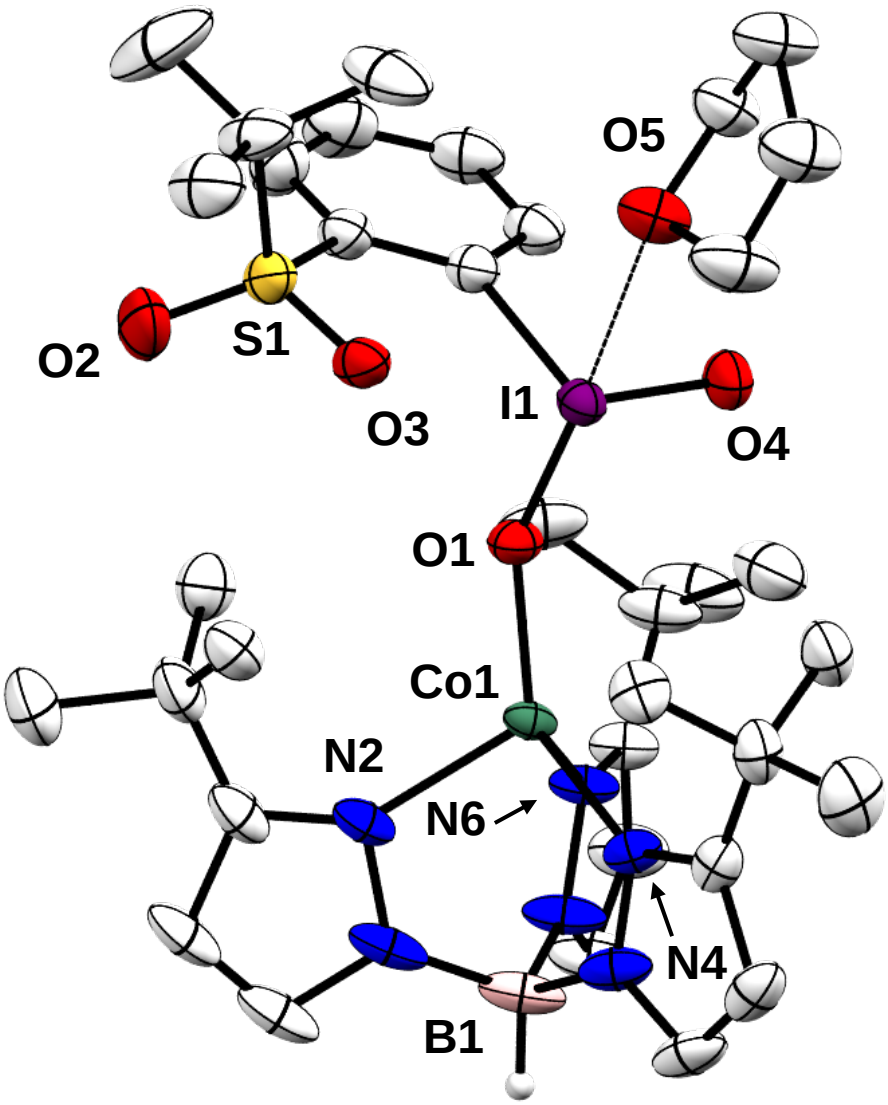

Figure S41. Structure of **3** showing the secondary interaction of a THF molecule with the iodine center of the bound $^{s}PhIO_2$ ligand. The I1-O5 distance is 2.558(4) Å. Thermal ellipsoids shown at 50% probability and counter anion, other solvent, and H-atoms other than B-H omitted for clarity.

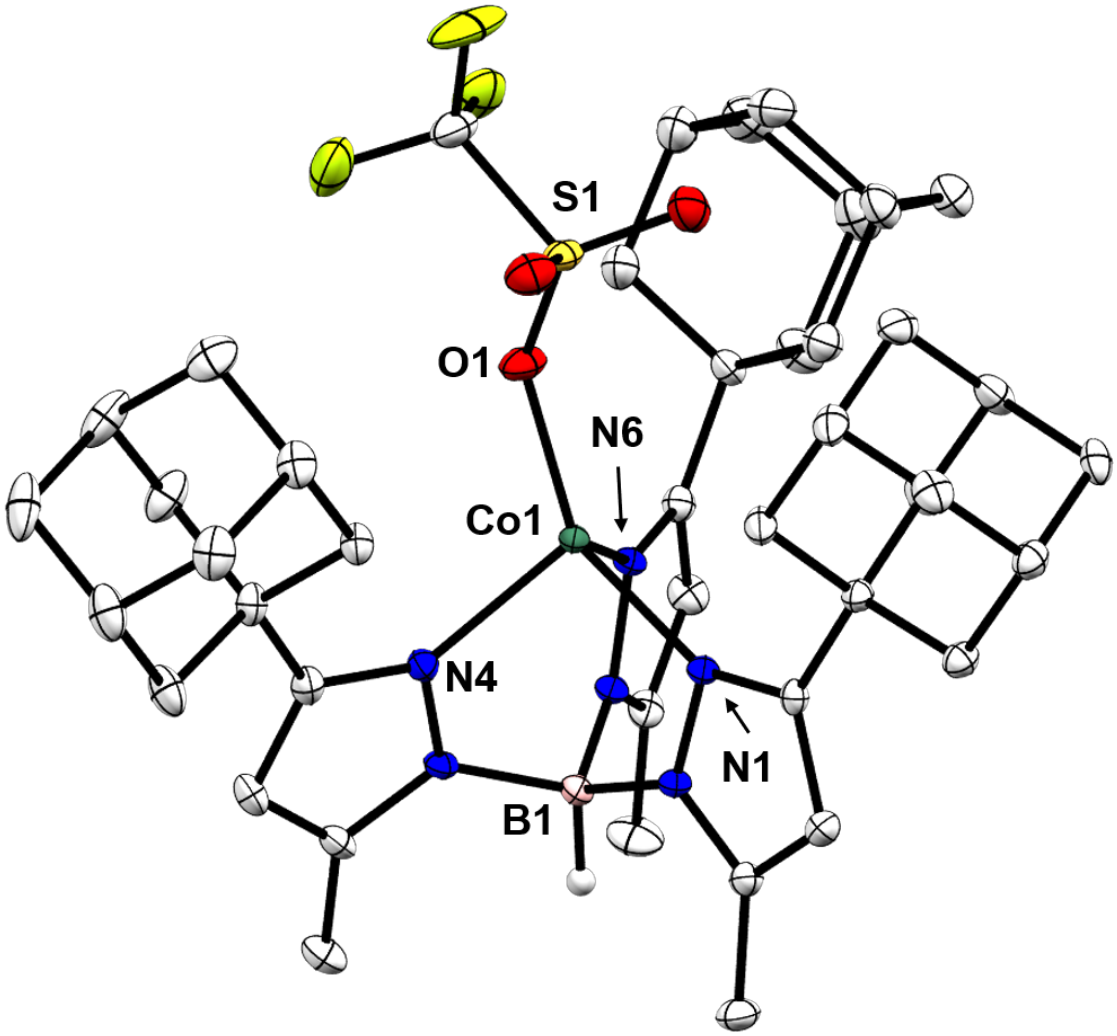

Figure S42. Depiction of the molecular structure of **4** determined by X-ray diffraction. Only one of the independent molecules is shown. Thermal ellipsoids shown at 50% probability. H-atoms other than B-H have been omitted for clarity.

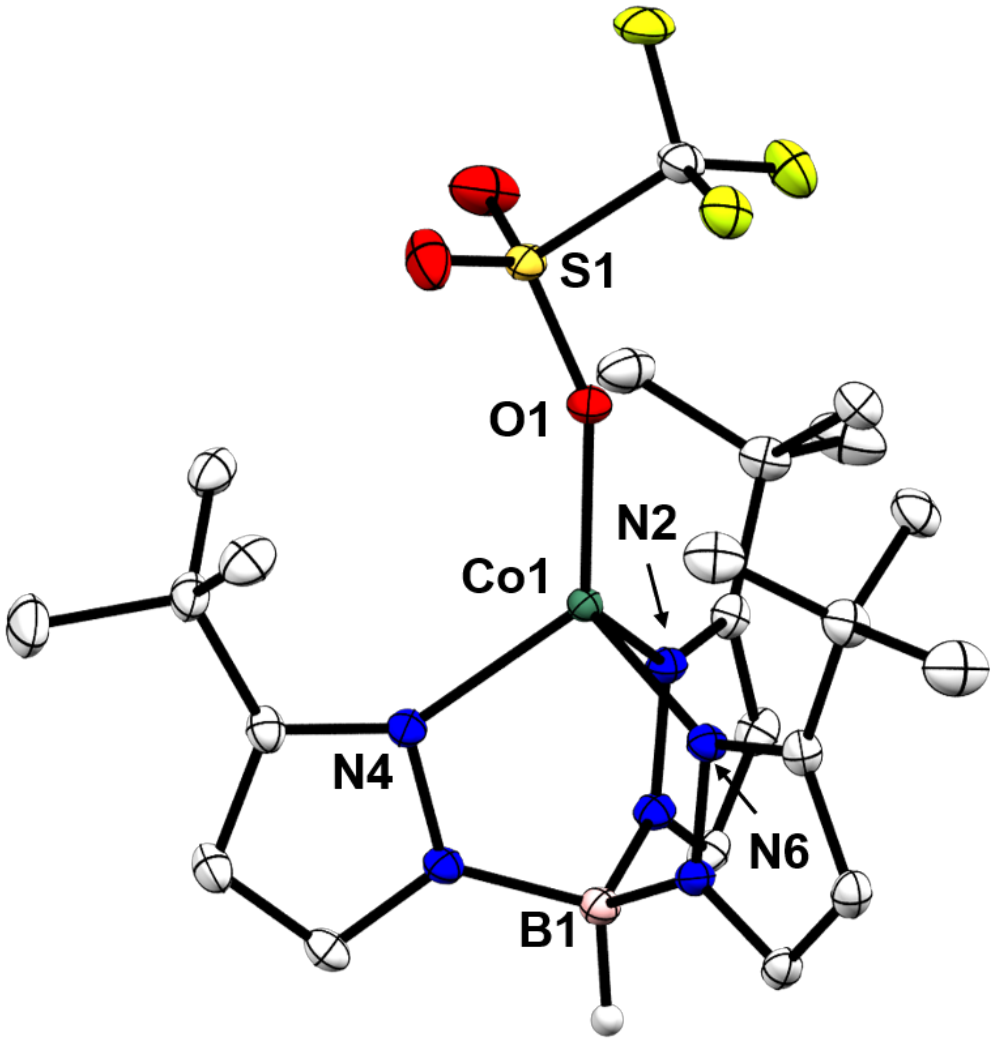

Figure S43. Depiction of the molecular structure of **5** determined by X-ray diffraction. Thermal ellipsoids shown at 50% probability. H-atoms other than B-H and a Et_2O molecule have been omitted for clarity.

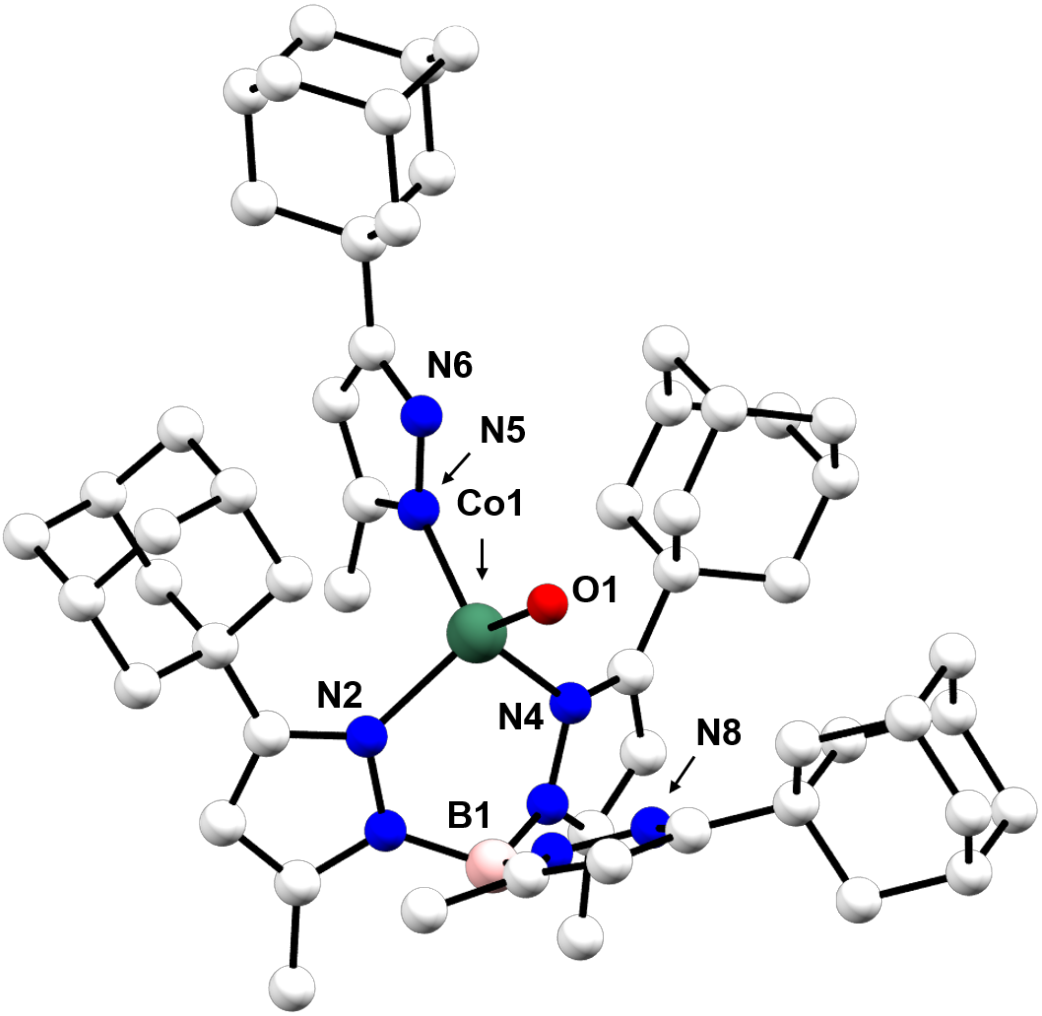

Figure S44. Depiction of the molecular structure of **6** determined by X-ray diffraction. Shown as ball and stick model for connectivity only. Atom labeled O1 is from coordinated OTf. The H-atoms, disordered Et_2O solvent molecule, and BAr^F_4 counter ion omitted for clarity.

4.3 Metrical Parameters

Table S5: Selected bond distances and angles for the Co complexes reported.

Complex:	**1**	**2**	**3**	**4**	**5**	**6**
Bond Length (Å)						
Co1-N_{avg}	2.037	2.032	2.026	2.038	2.016	2.027
Co1-O1	1.920(6)	1.934(3)	1.925(3)	1.955(1)	1.948(1)	1.994(2)
I1-O1	1.878(6)	1.891(3)	1.814(3)	N/A	N/A	N/A
I1-O4	N/A	N/A	1.780(3)	N/A	N/A	N/A
Angle (°)						
B1-Co1-O1	160.4(3)	171.6(1)	173.7(1)	161.11(5)	175.59(4)	107.1(2)

4.4 Refinement Details

Table S6. Crystal data and structure refinement for 1.

Identification code	1
Empirical formula	$C_{169}H_{168}B_4Cl_2Co_2F_{48}I_2N_{12}O_6S_2$
Formula weight	3925.06
Temperature/K	100(2)
Crystal system	triclinic
Space group	P-1
a/Å	14.2995(9)
b/Å	16.0821(11)
c/Å	38.551(3)
α/°	95.079(2)
β/°	97.357(2)
γ/°	97.863(2)
Volume/Å^3	8658.9(10)
Z	2
ρ_{calc}g/cm^3	1.505
μ/mm^{-1}	0.713
F(000)	3984.0
Crystal size/mm^3	0.33 × 0.24 × 0.12
Radiation	MoKα (λ = 0.71073)
2Θ range for data collection/°	4.328 to 50.14
Index ranges	$-15 \le h \le 16$, $-19 \le k \le 18$, $-45 \le l \le 45$
Reflections collected	86794
Independent reflections	29336 [R_{int} = 0.1033, R_{sigma} = 0.1379]
Data/restraints/parameters	29336/363/2310
Goodness-of-fit on F^2	1.068
Final R indexes [I>=2σ (I)]	R_1 = 0.0887, wR_2 = 0.1610
Final R indexes [all data]	R_1 = 0.1561, wR_2 = 0.1833
Largest diff. peak/hole / e Å^{-3}	1.26/-0.94

$R_{int} = \Sigma \mid F_o^2 - \langle F_o^2 \rangle \mid / \Sigma \mid F_o^2 \mid$

$R1 = \Sigma \mid \mid F_o \mid - \mid F_c \mid \mid / \Sigma \mid F_o \mid$

$wR2 = [\Sigma [w (F_o^2 - F_c^2)^2] / \Sigma [w (F_o^2)^2]]^{1/2}$

Goodness-of-fit = $[\Sigma [w (F_o^2 - F_c^2)^2] / (n-p)]^{1/2}$

n: number of independent reflections; p: number of refined parameters

Table S7. Crystal data and structure refinement for 2.

Identification code	2
Empirical formula	$C_{63}H_{59}B_2CoF_{24}IN_6O_3S$
Formula weight	1643.67
Temperature/K	100(2)
Crystal system	triclinic
Space group	P1
a/Å	10.4248(7)
b/Å	12.9027(9)
c/Å	15.4799(11)
α/°	101.302(2)
β/°	105.089(2)
γ/°	113.446(2)
Volume/Å^3	1735.7(2)
Z	1
ρ_{calc}g/cm^3	1.572
μ/mm^{-1}	0.835
F(000)	825.0
Crystal size/mm^3	0.25 × 0.15 × 0.05
Radiation	MoKα (λ = 0.71073)
2Θ range for data collection/°	4.308 to 55.12
Index ranges	-13 ≤ h ≤ 13, -16 ≤ k ≤ 16, -20 ≤ l ≤ 20
Reflections collected	49488
Independent reflections	15013 [R_{int} = 0.0272, R_{sigma} = 0.0384]
Data/restraints/parameters	15013/3/926
Goodness-of-fit on F^2	1.036
Final R indexes [I>=2σ (I)]	R_1 = 0.0256, wR_2 = 0.0518
Final R indexes [all data]	R_1 = 0.0290, wR_2 = 0.0528
Largest diff. peak/hole / e Å^{-3}	0.60/-0.38
Flack parameter	-0.012(3)

$R_{int} = \Sigma \mid F_o^2 - \langle F_o^2 \rangle \mid / \Sigma \mid F_o^2 \mid$

$R1 = \Sigma \mid \mid F_o \mid - \mid F_c \mid \mid / \Sigma \mid F_o \mid$

$wR2 = [\Sigma [w (F_o^2 - F_c^2)^2] / \Sigma [w (F_o^2)^2]]^{1/2}$

Goodness-of-fit = $[\Sigma [w (F_o^2 - F_c^2)^2] / (n-p)]^{1/2}$

n: number of independent reflections; p: number of refined parameters

Table S8. Crystal data and structure refinement for 3.

Identification code	3
Empirical formula	$C_{71}H_{77}B_2CoF_{24}IN_6O_6S$
Formula weight	1805.89
Temperature/K	100(2)
Crystal system	triclinic
Space group	P-1
a/Å	13.018(3)
b/Å	17.299(4)
c/Å	19.933(4)
α/°	69.338(4)
β/°	77.588(5)
γ/°	78.279(5)
Volume/Å^3	4062.0(14)
Z	2
ρ_{calc}g/cm^3	1.477
μ/mm^{-1}	0.178
F(000)	1830.0
Crystal size/mm^3	0.004 × 0.003 × 0.003
Radiation	synchrotron (λ = 0.41328)
2Θ range for data collection/°	1.478 to 32.428
Index ranges	$-17 \leq h \leq 17$, $-23 \leq k \leq 23$, $-26 \leq l \leq 26$
Reflections collected	114410
Independent reflections	19783 [R_{int} = 0.0498, R_{sigma} = 0.0327]
Data/restraints/parameters	19783/136/1055
Goodness-of-fit on F^2	1.022
Final R indexes [I>=2σ (I)]	R_1 = 0.0624, wR_2 = 0.1946
Final R indexes [all data]	R_1 = 0.0670, wR_2 = 0.1990
Largest diff. peak/hole / e Å^{-3}	2.23/-2.11

$R_{int} = \Sigma \mid F_o^2 - \langle F_o^2 \rangle \mid / \Sigma \mid F_o^2 \mid$

$R1 = \Sigma \mid \mid F_o \mid - \mid F_c \mid \mid / \Sigma \mid F_o \mid$

$wR2 = [\Sigma [w (F_o^2 - F_c^2)^2] / \Sigma [w (F_o^2)^2]]^{1/2}$

Goodness-of-fit = $[\Sigma [w (F_o^2 - F_c^2)^2] / (n-p)^{1/2}$

n: number of independent reflections; p: number of refined parameters

Table S9. Crystal data and structure refinement for 4.

Identification code	4
Empirical formula	$C_{43}H_{58}BCoF_3N_6O_3S$
Formula weight	865.75
Temperature/K	100(2)
Crystal system	triclinic
Space group	P-1
a/Å	11.3925(6)
b/Å	16.9868(8)
c/Å	21.7195(11)
α/°	94.871(2)
β/°	98.674(2)
γ/°	92.305(2)
Volume/Å^3	4134.1(4)
Z	4
ρ_{calc}g/cm^3	1.391
μ/mm^{-1}	0.527
F(000)	1828.0
Crystal size/mm^3	0.36 × 0.22 × 0.15
Radiation	MoKα (λ = 0.71073)
2Θ range for data collection/°	4.242 to 56.798
Index ranges	$-15 \leq h \leq 15$, $-22 \leq k \leq 22$, $-29 \leq l \leq 29$
Reflections collected	183013
Independent reflections	20681 [R_{int} = 0.0466, R_{sigma} = 0.0279]
Data/restraints/parameters	20681/0/1057
Goodness-of-fit on F^2	1.030
Final R indexes [I>=2σ (I)]	R_1 = 0.0411, wR_2 = 0.0979
Final R indexes [all data]	R_1 = 0.0646, wR_2 = 0.1106
Largest diff. peak/hole / e Å^{-3}	0.77/-0.43

$R_{int} = \Sigma \mid F_o^2 - \langle F_o^2 \rangle \mid / \Sigma \mid F_o^2 \mid$

$R1 = \Sigma \mid \mid F_o \mid - \mid F_c \mid \mid / \Sigma \mid F_o \mid$

$wR2 = [\Sigma [w (F_o^2 - F_c^2)^2] / \Sigma [w (F_o^2)^2]]^{1/2}$

Goodness-of-fit = $[\Sigma [w (F_o^2 - F_c^2)^2] / (n-p)]^{1/2}$

n: number of independent reflections; p: number of refined parameters

Table S10. Crystal data and structure refinement for 5.

Identification code	5
Empirical formula	$C_{26}H_{44}BCoF_3N_6O_4S$
Formula weight	663.47
Temperature/K	100(2)
Crystal system	monoclinic
Space group	$P2_1/n$
a/Å	10.4361(10)
b/Å	20.2414(18)
c/Å	15.3862(14)
α/°	90
β/°	91.209(3)
γ/°	90
Volume/Å^3	3249.5(5)
Z	4
ρ_{calc}g/cm^3	1.356
μ/mm^{-1}	0.650
F(000)	1396.0
Crystal size/mm^3	0.45 × 0.3 × 0.1
Radiation	MoKα (λ = 0.71073)
2Θ range for data collection/°	4.392 to 55.17
Index ranges	$-11 \le h \le 13$, $-26 \le k \le 26$, $-20 \le l \le 20$
Reflections collected	100848
Independent reflections	7508 [R_{int} = 0.0403, R_{sigma} = 0.0171]
Data/restraints/parameters	7508/0/394
Goodness-of-fit on F^2	1.045
Final R indexes [I>=2σ (I)]	R_1 = 0.0277, wR_2 = 0.0648
Final R indexes [all data]	R_1 = 0.0337, wR_2 = 0.0673
Largest diff. peak/hole / e Å^{-3}	0.44/-0.32

$R_{int} = \Sigma \mid F_o^2 - \langle F_o^2 \rangle \mid / \Sigma \mid F_o^2 \mid$

$R1 = \Sigma \mid \mid F_o \mid - \mid F_c \mid \mid / \Sigma \mid F_o \mid$

$wR2 = [\Sigma [w (F_o^2 - F_c^2)^2] / \Sigma [w (F_o^2)^2]]^{1/2}$

Goodness-of-fit = $[\Sigma [w (F_o^2 - F_c^2)^2] / (n-p)^{1/2}$

n: number of independent reflections; p: number of refined parameters

Table S11. Crystal data and structure refinement for 6.

Identification code	6
Empirical formula	$C_{93}H_{100}B_2CoF_{27}N_8O_4S$
Formula weight	2019.41
Temperature/K	100(2)
Crystal system	orthorhombic
Space group	Pbca
a/Å	21.4930(17)
b/Å	22.3378(19)
c/Å	38.715(3)
α/°	90
β/°	90
γ/°	90
Volume/Å^3	18587(3)
Z	8
ρ_{calc}g/cm^3	1.443
μ/mm^{-1}	0.317
F(000)	8336.0
Crystal size/mm^3	0.35 × 0.15 × 0.1
Radiation	MoKα (λ = 0.71073)
2Θ range for data collection/°	4.206 to 49.632
Index ranges	-25 ≤ h ≤ 25, -26 ≤ k ≤ 26, -45 ≤ l ≤ 45
Reflections collected	251224
Independent reflections	16006 [R_{int} = 0.1273, R_{sigma} = 0.0598]
Data/restraints/parameters	16006/58/1213
Goodness-of-fit on F^2	1.023
Final R indexes [I>=2σ (I)]	R_1 = 0.1073, wR_2 = 0.2609
Final R indexes [all data]	R_1 = 0.1568, wR_2 = 0.2964
Largest diff. peak/hole / e Å^{-3}	2.92/-2.37

$R_{int} = \Sigma \mid F_o^2 - \langle F_o^2 \rangle \mid / \Sigma \mid F_o^2 \mid$

$R1 = \Sigma \mid \mid F_o \mid - \mid F_c \mid \mid / \Sigma \mid F_o \mid$

$wR2 = [\Sigma [w (F_o^2 - F_c^2)^2] / \Sigma [w (F_o^2)^2]]^{1/2}$

Goodness-of-fit = $[\Sigma [w (F_o^2 - F_c^2)^2] / (n-p)^{1/2}$

n: number of independent reflections; p: number of refined parameters

5.0 References

[1] D. Macikenas, E. Skrzypczak-Jankun, J. D. Protasiewicz, *J. Am. Chem. Soc.* **1999**, *121*, 7164–7165.
[2] F. Song, C. Wang, J. M. Falkowski, L. Ma, W. Lin, *J. Am. Chem. Soc.* **2010**, *132*, 15390–15398.
[3] R. J. Angelici, Ed. , *Inorganic Syntheses*, John Wiley & Sons, Inc., Hoboken, NJ, USA, **1990**.
[4] C. Goldsmith, R. Jonas, T. Stack, *J. Am. Chem. Soc.* **2002**, *124*, 83–96.
[5] A. McSkimming, W. H. Harman, *J. Am. Chem. Soc.* **2015**, *137*, 8940–8943.
[6] N. Chakrabarti, W. Sattler, G. Parkin, *Polyhedron* **2013**, *58*, 235–246.
[7] D. Macikenas, E. Skrzypczak-Jankun, J. D. Protasiewicz, *Angew. Chem. Int. Ed.* **2000**, *39*, 2007–2010.
[8] L. Krause, R. Herbst-Irmer, G. M. Sheldrick, D. Stalke, *J. Appl. Crystallogr.* **2015**, *48*, 3–10.
[9] G. M. Sheldrick, *Acta Crystallogr.* **2015**, *A71*, 3–8.
[10] O. V. Dolomanov, L. J. Bourhis, R. J. Gildea, J. A. K. Howard, H. Puschmann, *J. Appl. Crystallogr.* **2009**, *42*, 339–341.
[11] G. M. Sheldrick, *Acta Crystallogr.* **2015**, *C71*, 3–8.